Journal of Anatomy

J. Anat. (2015) **227**, pp611–630 doi: 10.1111/joa.12367

Bone histology in extant and fossil penguins (Aves: Sphenisciformes)

Daniel T. Ksepka,[1,2] Sarah Werning,[3]* Michelle Sclafani[4] and Zachary M. Boles[5]

[1]*Bruce Museum, Greenwich, CT, USA*
[2]*Smithsonian National Museum of Natural History, Washington, DC, USA*
[3]*Department of Anatomical Sciences, Stony Brook University, Stony Brook, NY, USA*
[4]*North Carolina Department of Environment and Natural Resources, Raleigh, NC, USA*
[5]*Department of Biology, Drexel University, Philadelphia, PA, USA*

Abstract

Substantial changes in bone histology accompany the secondary adaptation to life in the water. This transition is well documented in several lineages of mammals and non-avian reptiles, but has received relatively little attention in birds. This study presents new observations on the long bone microstructure of penguins, based on histological sections from two extant taxa (*Spheniscus* and *Aptenodytes*) and eight fossil specimens belonging to stem lineages (†*Palaeospheniscus* and several indeterminate Eocene taxa). High bone density in penguins results from compaction of the internal cortical tissues, and thus penguin bones are best considered osteosclerotic rather than pachyostotic. Although the oldest specimens sampled in this study represent stages of penguin evolution that occurred at least 25 million years after the loss of flight, major differences in humeral structure were observed between these Eocene stem taxa and extant taxa. This indicates that the modification of flipper bone microstructure continued long after the initial loss of flight in penguins. It is proposed that two key transitions occurred during the shift from the typical hollow avian humerus to the dense osteosclerotic humerus in penguins. First, a reduction of the medullary cavity occurred due to a decrease in the amount of perimedullary osteoclastic activity. Second, a more solid cortex was achieved by compaction. In extant penguins and †*Palaeospheniscus*, most of the inner cortex is formed by rapid osteogenesis, resulting an initial latticework of woven-fibered bone. Subsequently, open spaces are filled by slower, centripetal deposition of parallel-fibered bone. Eocene stem penguins formed the initial latticework, but the subsequent round of compaction was less complete, and thus open spaces remained in the adult bone. In contrast to the humerus, hindlimb bones from Eocene stem penguins had smaller medullary cavities and thus higher compactness values compared with extant taxa. Although cortical lines of arrested growth have been observed in extant penguins, none was observed in any of the current sampled specimens. Therefore, it is likely that even these 'giant' penguin taxa completed their growth cycle without a major pause in bone deposition, implying that they did not undergo a prolonged fasting interval before reaching adult size.

Key words: bone microstructure; flightlessness; Spheniscidae; wing-propelled diving.

Introduction

George Gaylord Simpson proposed a three-stage theory of penguin evolution: an initial volant stage; a stage during which small-bodied early penguins were capable of both aerial flight and wing-propelled diving; and a final flightless wing-propelled diving stage (Simpson, 1946). Placing the acquisition of key morphological adaptations within the context of this three-stage model is key to understanding broad-scale patterns in the evolutionary history of penguins. Unfortunately, no fossil 'proto-penguins' from the first two stages have been recognized. Nonetheless, penguins have an extensive fossil record from the final flightless stage that, together with comparisons to extant penguins and outgroup taxa, can provide insight into the pattern of acquisition of the many derived features that these birds employ in underwater wing-propelled diving.

Among the myriad aquatic adaptations of penguins are pronounced modifications of bone structure. Meister (1962)

Correspondence
Daniel T. Ksepka, Bruce Museum, 1 Museum Drive, Greenwich, CT 06830, USA. E: dksepka@brucemuseum.org

**Current Address: Department of Anatomy, Des Moines University, Des Moines, IA, USA*

Accepted for publication *17 July 2015*
Article published online *11 September 2015*

provided the first detailed account of extant penguin bone histology, based on captive zoo specimens of *Pygoscelis adeliae* (Adélie Penguin), *Aptenodytes forsteri* (Emperor Penguin) and *Aptenodytes patagonicus* (King Penguin). This work confirmed that extant penguin limb bones possess the thickest cortex observed among living birds. Penguin limb bones also differ from those of nearly all other birds in their greater bone density, near complete lack of pneumatization, unusually thick periosteum and greatly reduced medullary cavities (Meister, 1962). Chinsamy et al. (1998) later noted similarities in femoral histology between penguins (the Emperor Penguin and Black-footed Penguin, *Spheniscus demersus*) and those of two Cretaceous birds: the foot-propelled diving bird †*Hesperornis regalis* and the controversial †*Polarornis gregorii*, a taxon initially identified as a loon (Chatterjee, 2002) but now considered to be of uncertain affinity (e.g. Feduccia, 1999; Dyke & van Tuinen, 2004; Mayr et al. 2013). Most recently, Wilson & Chin (2014) provided descriptions of the histology of hindlimb elements of *Pygoscelis adeliae*, *Pygoscelis antarcticus* and *Pygoscelis papua*, and Cerda et al. (2015) provided a description of the histology of the tarsometatarsus of eight Eocene penguin fossils including several 'giant' taxa.

Dense bone commonly has been interpreted as a means of reducing buoyancy and thus conserving energy during diving (e.g. Nopcsa, 1923; Wall, 1983; Lovvorn et al. 1999). Additionally, increased thickness of the limb bone cortices can enhance resistance to bending or torsional loads, which are substantially higher in wing-propelled diving relative to most conditions encountered during aerial flight (Habib & Ruff, 2008). Because extant penguin wing bones exhibit cortical thickness far above that required for bending resistance alone, it is plausible that this increase in thickness serves both to increase ballast and to increase resistance (Habib, 2010). In order to address such hypotheses in an evolutionary context, it is important to determine whether penguins evolved a dense bone structure primarily during the initial acquisition of wing-propelled diving ecology, coincident with the loss of aerial flight, subsequent to the loss of aerial flight, or in stepwise fashion with shifts accompanying several of these evolutionary events.

Increased limb bone density can be achieved through a variety of mechanisms, the most commonly observed being pachyostosis and osteosclerosis (reviewed in de Ricqlès & de Buffrénil, 2001). Pachyostosis refers to hyperplasy of the periosteal bone. This results in thick, dense cortical bone and may also alter the shape of the bone as in the banana-shaped ribs of the mammalian Sirenia (Domning & de Buffrénil, 1991) and the distally expanded ribs of the diapsid Choristodera (Sigogneau-Russell, 1981). Osteosclerosis refers to increased bone mass in the innermost regions of the bone (de Ricqlès & de Buffrénil, 2001). This occurs either by thickening the inner circumferential layer (ICL), or by compaction of trabeculae through increased apposition and/or inhibited resorption (Domning & de Buffrénil, 1991; de Ricqlès & de Buffrénil, 2001). Osteosclerosis and pachyostosis can also co-occur (pachyosteosclerosis).

The bone structure of penguins has been variably referred to as pachyostotic (Meister, 1962; Mayr, 2005; Ksepka et al. 2006; Livezey & Zusi, 2006), osteosclerotic (de Ricqlès & de Buffrénil, 2001; Ksepka et al. 2008; Cerda et al. 2015) or pachyosteoscleortic (Houssaye, 2009). The term pachyostotic does not apply to penguins, because they do not exhibit periosteal hyperplasy: the external dimensions of the hind limb bones of penguins remain unexpanded, with hind limb bone cross-sectional area remaining within the range observed in similarly sized volant birds (DTK personal observation). Comparisons of the external dimensions of wing bones between penguins and volant birds are more difficult due to the highly flattened and shortened morphology of the penguin flipper. However, Meister (1962) demonstrated that the extremely high bone density of the penguin humerus is achieved solely through compaction of the internal tissues, without expansion of the external circumferential layer. This finding was further supported by observations from an ontogenetic series of *Aptenodytes patagonicus* specimens by Canoville (2010). Thus, the term 'osteosclerotic' is more accurately applied to penguin limb bones (de Ricqlès & de Buffrénil, 2001).

Beyond differences in bone structure, the skeletal growth patterns of penguins are unique in several ways. The King Penguin exhibits the fastest appositional bone growth rates that have been experimentally measured to date, reaching a maximum rate of 171 μm day^{-1} (de Margerie et al. 2004). This species is also one of the few crown avian taxa known to produce lines of arrested growth (LAGs): a single cortical LAG was reported in the femur of a ~1-year-old King Penguin chick (Castanet, 2006). Castanet (2006) considered it likely that this LAG was laid down during the fasting period of this species' unique life cycle. King Penguin chicks grow extremely rapidly for ~3 months before undergoing an ~4.5-month period of food deprivation when parental feeding slows dramatically during the austral winter. After this, feeding resumes and the chicks grow for ~3.5 months before molting and leaving the colony (Stonehouse, 1960; summarized in Williams, 1995). Emperor Penguin chicks also undergo periods of low food intake, but these are shorter and less intense than in King Penguins and apparently do not result in cortical LAG formation. Likewise, LAGs have not been observed in Antarctic *Pygoscelis* penguins (Wilson & Chin, 2014) or to the authors' knowledge any other extant penguin species other than King Penguins. In general, cortical LAGs are rare in crown avian taxa, although they have been observed in three extant kiwi species (*Apteryx*; Bourdon et al. 2009), the Orange-winged Amazon parrot (*Amazona amazonica*; figured in Amprino & Godina, 1947), the extinct Dinornithiformes (Moa; Turvey et al. 2005) and *Diatryma* (Padian et al. 2001).

In this paper, the bone microstructure of wild-caught or wild-salvaged (i.e. not captive) individuals of two extant penguin species and eight fossil specimens from outside the crown radiation were described (Spheniscidae; Figs 1 and 2). Including stem penguins opens up the possibility of sampling earlier stages in the evolution of penguin bone microstructure, prior to the acquisition of the present-day derived osteosclerotic condition. In addition to qualitative features of the bone tissues, two quantitative variables relating to bone density were considered: compactness and cortico-diaphyseal index (CDI; see Materials and methods for further descriptions). Phylogenetic trends in histology, compactness and CDI were examined in order to test whether these values differed significantly between stem and crown penguins.

Materials and methods

Institutional abbreviations

AMNH FARB – Fossil Reptile, Amphibian and Bird Collection, Department of Vertebrate Paleontology, American Museum of Natural History, New York, NY, USA; AMNH – Skeletal Collection, Department of Ornithology, American Museum of Natural History, New York, NY, USA; BRCM – Bruce Museum, Greenwich, CT, USA; UCMP – University of California Museum of Paleontology, Berkeley, CA, USA; UNCW – University of North Carolina Wilmington, NC,

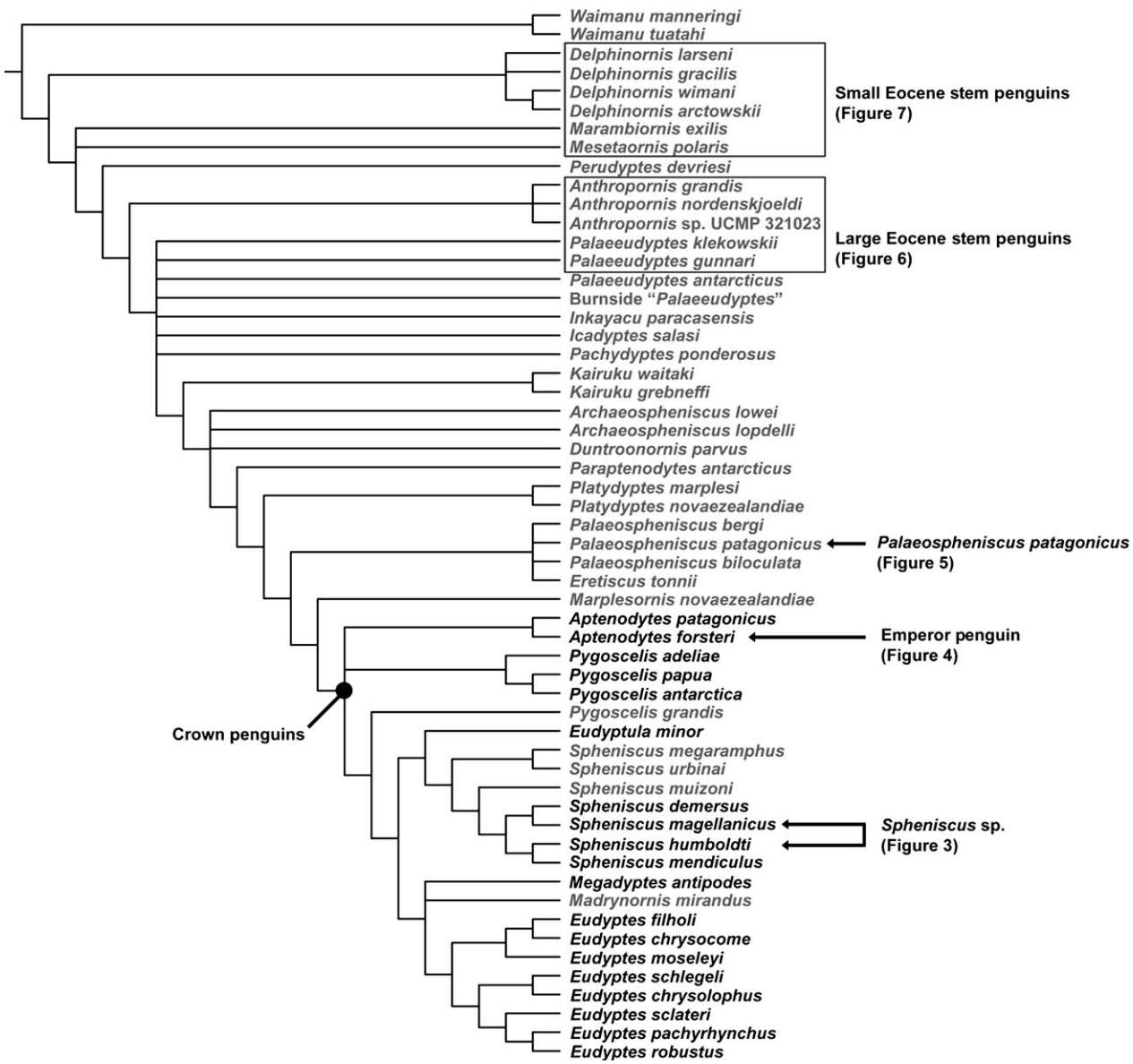

Fig. 1 Phylogeny of Sphenisciformes after Ksepka et al. (2012) indicating the specimens sampled in this study, with fossil taxa indicated in gray font. In the case of Eocene specimens from Seymour Island, size allows us to narrow down the possible species identities to those shown in the boxes. The *Spheniscus* specimen sampled here is either *Spheniscus magellanicus* or *Spheniscus humboldti*.

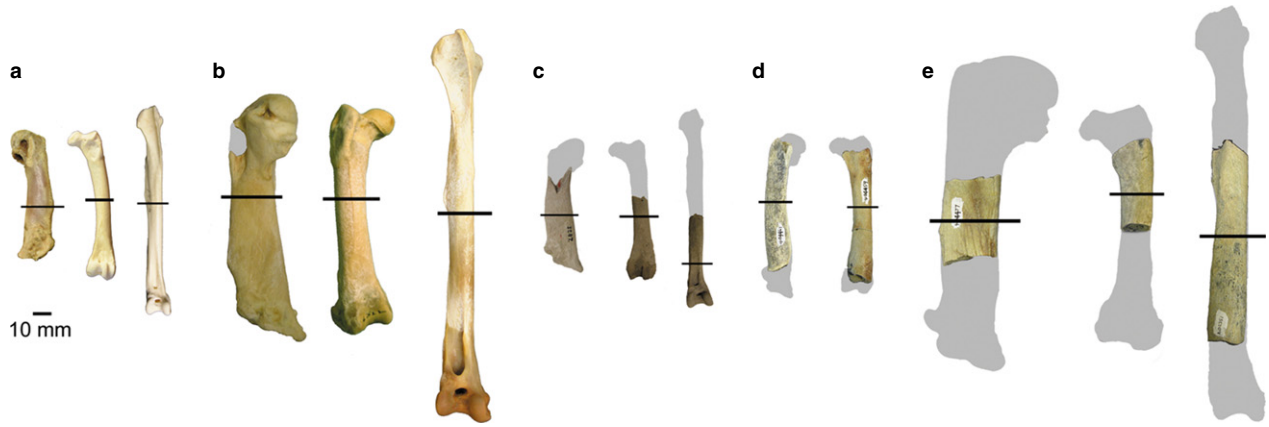

Fig. 2 Penguin specimens sampled in this study: (a) *Spheniscus* sp. (AMNH 1626) humerus, femur and tibiotarsus; (b) *Aptenodytes forsteri* (AMNH 3728) humerus, femur and tibiotarsus; (c) †*Palaeospheniscus patagonicus* humerus (AMNH FARB 3287), femur (AMNH FARB 3349) and tibiotarsus (AMNH FARB 3312); (d) small Eocene stem penguin humerus (USNM 404461) and femur (USNM 404459); (e) large Eocene stem penguin humerus (USNM 404477), femur (USNM 402616) and tibiotarsus (USNM 402351). Gray silhouettes indicate the approximate size of the complete elements, black lines indicate approximate point of sections illustrated in Figs 3–8. All elements are from the right side of the body.

USA; USNM – National Museum of Natural History, Smithsonian Institution, Washington, DC, USA.

Taxa and specimens

The bone microstructure, compactness and CDI of the humerus, femur and tibiotarsus from two extant penguins (*Aptenodytes forsteri* and *Spheniscus* sp.), three fossil stem penguins (†*Palaeospheniscus patagonicus* and two Eocene taxa) and the outgroups *Calonectris borealis* (Cory's Shearwater) and *Gavia immer* (Common Loon) were analyzed. A total of 20 long bone specimens were examined (see Table 1 for specimen numbers and Fig. 1 for phylogenetic relationships).

The extant species are each represented by a single adult individual. The skeletons of each of these represent wild-caught or wild-salvaged individuals, collected and accessioned into the AMNH Ornithology collections before 1935. Wild-collected specimens were used because of the high incidence of skeletal pathologies observed in skeletons of captive penguins (DTK personal observation). AMNH 1626, identified as *Spheniscus* sp., represents either *Spheniscus humboldti* (Humboldt Penguin) or *Spheniscus magellanicus* (Magellanic Penguin) based on size and collection locality (recorded only as Chile), though the precise identity was not determined when the skeleton was accessioned.

Complete fossil specimens (i.e. single individuals from an associated specimen) were not available for histological section-

Table 1 Specimens examined in this study.

Taxon	Specimen	Element	Length (mm)	Locality	Age
Aptenodytes forsteri	AMNH 3728	Humerus	125.5	Antarctica	Modern
Aptenodytes forsteri	AMNH 3728	Femur	122.2	Antarctica	Modern
Aptenodytes forsteri	AMNH 3728	Tibiotarsus	198.6	Antarctica	Modern
Spheniscus sp.	AMNH 1626	Humerus	71.7	Chile	Modern
Spheniscus sp.	AMNH 1626	Femur	82.8	Chile	Modern
Spheniscus sp.	AMNH 1626	Tibiotarsus	114.3	Chile	Modern
†*Palaeospheniscus patagonicus*	AMNH 3287	Humerus	~75	Gaiman Fm., Argentina	Miocene
†*Palaeospheniscus patagonicus*	AMNH 3349	Femur	~84	Gaiman Fm., Argentina	Miocene
†*Palaeospheniscus patagonicus*	AMNH 3321	Tibiotarsus	~110	Gaiman Fm., Argentina	Miocene
†Small Eocene stem penguin	USNM 404461	Humerus	~80	La Meseta Fm., Antarctica	Eocene
†Small Eocene stem penguin	USNM 404459	Femur	~90	La Meseta Fm., Antarctica	Eocene
†Large Eocene stem penguin	USNM 404477	Humerus	~160	La Meseta Fm., Antarctica	Eocene
†Large Eocene stem penguin	USNM 402616	Femur	~130	La Meseta Fm., Antarctica	Eocene
†Large Eocene stem penguin	USNM 402351	Tibiotarsus	~225	La Meseta Fm., Antarctica	Eocene
Calonectris borealis	BRCM 2015.04	Humerus	133.4	North Carolina, USA	Modern
Calonectris borealis	BRCM 2015.04	Femur	44.9	North Carolina, USA	Modern
Calonectris borealis	BRCM 2015.04	Tibiotarsus	97.5	North Carolina, USA	Modern
Gavia immer	BRCM 2015.03	Humerus	Incomplete	Unknown	Modern
Gavia immer	BRCM 2015.03	Femur	Incomplete	Unknown	Modern
Gavia immer	BRCM 2015.03	Tibiotarsus	Incomplete	Unknown	Modern

ing, so partial long bones were selected. Bones of the stem penguin †*Palaeospheniscus patagonicus* from the Miocene Gaiman Formation of Argentina were identified to the species level based on comparisons with complete specimens from the same locality.

Two 'small' Eocene specimens were sampled, both from the Late Eocene La Meseta Formation of Seymour Island, Antarctica. These fossils were collected in isolation and were originally deposited in an estuarine setting (Porębski, 1995), and are ~34.7–36.1 Ma in age (Dutton et al. 2002). Incompleteness precludes species level identifications for these specimens, although this can at least be narrowed to a few taxa. The small Eocene penguins sampled here could potentially represent any of five species: †*Delphinornis arctowskii*; †*Delphinornis larseni*; †*Delphinornis gracilis*; †*Mesetaornis polaris*; and †*Marambiornis exilis* (see Myrcha et al. 2002 and Jadwiszczak, 2006 for an overview of this species assemblage). A finer identification is not possible because these taxa are each based on tarsometatarsus holotypes and associated skeletons are lacking (see Ksepka & Clarke, 2010 for further discussion). Fortuitously, all of these species are placed on basal branches in the cladogram (Fig. 1). Although they are referred to as 'small' to distinguish them from the more commonly recovered giant penguin taxa of the La Meseta Formation, the penguins sampled were comparable in size to moderate-sized extant taxa (i.e. *Pygoscelis adeliae*) based on limb bone measurements (Jadwiszczak, 2001). Based on the dimensions and development of observable muscle insertions, these appear to all belong to adult taxa.

Also, three 'large' (exceeding Emperor Penguin in comparable dimensions) fossil specimens from the same site were sampled. The humerus (USNM 404477) could belong to one of three taxa based on preserved morphologies and size: †*Anthropornis nordenskjoeldi*, †*Anthropornis grandis* or †*Palaeeudyptes klekowskii*. The tibiotarsus and femur could belong to any of those three species or to †*Palaeeudyptes gunnari*. These four stem species also occupy a narrow phylogenetic interval far outside of Spheniscidae (Fig. 1), although they represent more crownward branches than the small La Meseta taxa. In addition to broadening the phylogenetic sample to include stem penguins, the current dataset includes taxa that are far outside the size range of any living species, which potentially exhibited different diving habits and/or growth strategies.

Specimen preparation

Three bones were selected for sampling for each taxon: the humerus, femur and tibiotarsus (Table 1). The mid-point of the shaft (50% total length) was sampled in each element when possible. For incomplete bones, the mid-diaphysis was estimated by comparison to complete elements of the same size. For two bones, incompleteness resulted in an offset from the midpoint: for the †*Palaeospheniscus patagonicus* tibiotarsus (AMNH FARB 3321), the proximal-most preserved portion of the element was sampled (inferred to be distal to the mid-point); and for large Eocene penguin femur (USNM 402616), slightly proximal to inferred mid-point was sampled to obtain an intact section of the partial bone (Fig. 2).

Canoville (2010) observed that in *Aptenodytes patagonicus*, the mid-diaphysis lies at 56% of the total (i.e. proximo-distal) length in the humerus, at 54% in the femur and at 65–70% in the tibiotarsus (measured from the proximal end in all cases). The current 50% sampling location likely closely approximates mid-diaphysis in the humerus and femur. This is confirmed by the presence of the nutrient canal in the bone wall or confluent with the medullary cavity in the slides of most of the humeri and femora (e.g. Fig. 6). This canal houses the arterial supply for the primary diaphyseal growth center during development, and marks the position of mid-diaphysis in adults (Payton, 1934). The nutrient canal is visible at 50% total length in the tibiotarsus of *Spheniscus* sp. (Fig. 3), suggesting that the mid-diaphysis lies more proximally in this taxon than in *A. patagonicus*. A nutrient canal is also visible in the tibiotarsus of †*Palaeospheniscus* (Fig. 5), which was sampled much more distally (Fig. 2c). The position of the tibiotarsal mid-diaphysis seems to vary among penguins, and thus the current typical 50% sampling location may not represent mid-diaphysis in some cases.

All specimens were skeletonized or removed from their rock matrix prior to the study. In order to enable direct comparisons with fossil bone, recent specimens were not decalcified prior to sectioning. Samples were removed and embedded in a 25 : 3 by volume mixture of Epofix Resin and Epofix Hardener (Struers, Cleveland, OH, USA) and allowed to cure. The embedded specimens were then sectioned using an IsoMet Low Speed Saw (Buehler, Lake Bluff, IL, USA). Most sections were polished using a rotating polisher with a sequence of P400, P1200, P2400 and P4000 grit abrasive papers sequentially. Alternatively, several sections were polished using 70 μm flat, 10 μm flat and 2 μm polish abrasive discs sequentially. The polished side of each section was then mounted onto a glass slide using a 5 : 1 by weight mixture of EpoThin Low Viscosity Epoxy Resin and EpoColor Hardener (Buehler). The other side of the section was then ground and polished to ~100 μm thickness using the same procedure as above. For the outgroup taxa, specimens were embedded using Silmar resin (Interplastic, St Paul, MN, USA), sectioned using a Buehler Isomet 1000 Precision Saw and polished using a EcoMet 4000 Variable Speed Grinder-Polisher (Buehler). The polished side of each slide was mounted using Loctite Epoxy Instant Mix Five Minute (Henkel, Westlake, OH, USA), and the other side of the section was then ground and polished to ~100 μm thickness.

Data collection and analysis

The program Bone Profiler 3.23 (Girondot & Laurin, 2003) was used to estimate CDI and compactness values for each section. CDI is calculated as the thickness of the cortex of the bone divided by the radius of the bone (Castanet et al. 2000). Compactness (a measure of the amount and distribution of bone present) was chosen as a proxy for bone density, which is one of the most important properties of bone from a functional standpoint. It was not possible to measure bone density directly in this study, because it is a product of both mineral density and the volume/area of bone present. Original mineral density cannot be accurately obtained from fossilized bone (Germain & Laurin, 2005), but compactness values are directly comparable between recent and fossil samples, and is thus an appropriate proxy for the current study. Compactness provides an overall proxy of density of a given section of bone, taking into account the presence and density of trabecular bone in the medullary cavity, whereas CDI provides a measure of bone cortex thickness, ignoring properties of the medullary cavity. Both values have been applied to studies of extinct organisms (e.g. Canoville & Laurin, 2010; Hayashi et al. 2013; Meier et al. 2013; Straehl et al. 2013).

To estimate these values using Bone Profiler, each slide was scanned using a flatbed scanner. Because Bone Profiler distinguishes bone from open space based on pixel color, areas such as mineral deposits and matrix infill were digitally removed from the scans using photoshop cs (Adobe Systems, San Jose, CA, USA) to prevent

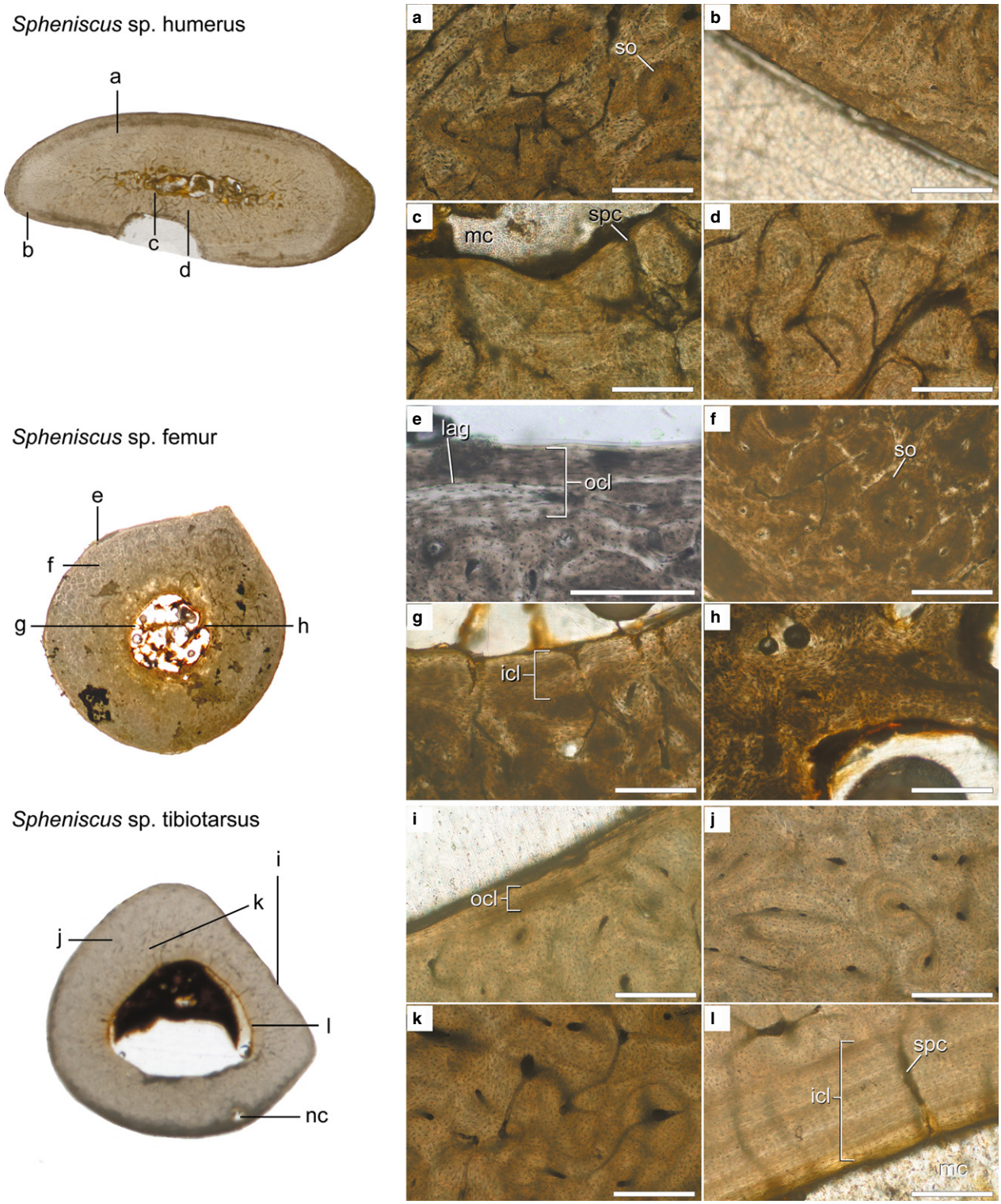

Fig. 3 Histological cross-sections from the mid-diaphyses of *Spheniscus* sp. (AMNH 1626) limb elements. Scanned images of the entire sections (not to scale) are shown at the left and microscope images of key regions of the sections are shown at the right (a–l). Cross-section scans are orientated so that the caudal surface of the humerus and the cranial surfaces of the femur and tibiotarsus face the top of the page. A missing section of the humerus is due to specimen damage. Scale bars: 250 μm (a–l). Abbreviations: icl, inner circumferential layer; lag, line of arrested growth; mc, medullary cavity; nc, nutrient canal; ocl, outer circumferential layer; so, secondary osteon; spc, simple primary canal.

them from being mistakenly identified as bone. Then, the photographs were converted into binary images using PHOTOSHOP CS by converting pixels representing bone to black and pixels representing open spaces to white. Automatic centering was used for all slides except the large Eocene humerus (USNM 404477). For this specimen, BONE PROFILER placed the bone center within the compacta due to the displacement of the medullary cavity, and so the center of the medullary cavity was manually specified to avoid underestimation of CDI. The compactness and CDI datasets were supplemented by including four *Pygoscelis* hind limb elements sampled by Wilson & Chin (2014) using their high-resolution composite cross-sectional images (available at Morphobank, Project 1270: http://dx.doi.org/10.7934/P1270).

Histological observations were made by eye through transmitted light microscopes, and described using the terminology of Francillon-Vieillot et al. (1990) and de Ricqlès & de Buffrénil (2001). Descriptions proceed from the endosteal margin towards the periosteal margin. Detailed histological images were collected with microscope-mounted digital cameras. Original high-resolution histological images are reposited online at MorphoBank (Project 1111, http://morphobank.org/permalink/?P1111).

Histological descriptions

In the descriptions below, standard orientation were used for avian bones (Baumel & Witmer, 1993). This corresponds to the orientation of the flipper in a standing penguin, as opposed to the orientation in a swimming bird. Thus, for example, the surface of the humerus facing cranially in a standing penguin with outstretched flippers is referred to as cranial, whereas it would be considered ventral in the context of a swimming bird (e.g. in many early descriptions such as Marples, 1952).

Spheniscus sp.

The humerus of *Spheniscus* is characterized by thick, densely vascularized woven-fibered cortical bone and a small, compacted medullary cavity (Fig. 3, top cross-section). The oval medullary cavity is strikingly different from the typical avian condition in both its greatly reduced area and its highly compressed shape. Meister (1962) referred to this region as the 'marrow area' to distinguish it from the open medullary cavity of other birds, but this study uses the homologous term for clarity. At mid-diaphysis, the medullary cavity is centrally located, but in more distal portions of the shaft it is displaced towards the ventral margin. At the microstructural level, the endosteal margin differs from that of most birds in lacking a distinct, continuous ICL, although parallel-fibered bone is present along some parts of the margin (Fig. 3c). In some areas, the vascular canals of the cortex end abruptly at the endosteal margin (Fig. 3c). In other areas, thick trabeculae extend into or across the medullary cavity, giving it a chambered appearance in cross-section (Fig. 3, top cross-section).

The cortex is composed of well-vascularized, primary woven-fibered bone tissue. Longitudinal secondary osteons are present in only a few localized regions (Fig. 3a), but most vascular canals are either primary osteons or simple canals. These form a reticular pattern throughout most of the cortex (Fig. 3a), but radial patterns occur in some areas (Fig. 3, top cross-section). Dense reticular vascularization continues throughout most of the cortex, but the bone abruptly transitions to poorly vascularized, parallel-fibered bone tissue close to the periosteal surface. This thin layer is present around most of the humeral circumference, but a true outer circumferential layer (OCL) of lamellar bone is absent (Fig. 3b).

The femur is characterized by an extremely thick cortex and a small, clearly defined medullary cavity (Fig. 3, middle cross-section). A thin ICL of centripetally deposited lamellar bone forms most of the endosteal border (Fig. 3g). A few rather large trabeculae enter the cavity but do not span it. They do delimit a few small interstitial spaces, contrary to previous observations for this genus by Chinsamy et al. (1998). Most of the cortex is secondarily remodeled (Fig. 3f), but small patches of primary woven-fibered bone are occasionally visible between the longitudinal secondary osteons. The cortex of the femur makes up ~75% of bone diameter, higher than previous measurements from a *Spheniscus demersus* femur (62%; Chinsamy et al. 1998). Determining whether this reflects ontogenetic, individual or interspecific variation requires further sampling. An OCL of avascular lamellar bone is distinct from the cortex and divided into two layers by a rest line (Fig. 3e) that travels around most of the circumference. Rest lines are relatively common in the OCL of birds (Chinsamy-Turan, 2005), but their utility for skeletochronology is incompletely understood.

The tibiotarsus is subtriangular in cross-section, and the medullary cavity is larger than in the humerus and femur and also lacks trabeculae (Fig. 3, lower cross-section). The most notable feature is the ICL of centripetal bone lining the medullary cavity (Fig. 3l), which is very thick on the cranial margin of the cavity but absent on the caudal margin. Radial simple primary canals traverse the ICL and extend into the cortex, where they anastomose with other canals (Fig. 3l). The cortex is fairly uniform, composed mainly of woven-fibered bone. Here, the primary osteons are predominately longitudinal or oblique in a single transverse plane, but focusing through the section shows that they form three-dimensional reticulations (Fig. 3k). Very few small secondary osteons are present, and the OCL is very thin (Fig. 3i). Unlike the femur, no rest line is present within the OCL of the tibiotarsus.

Aptenodytes forsteri

The humeral microstructure of *Aptenodytes forsteri* shares many features with that of *Spheniscus*. The largest differences concern the medullary cavity, which is almost completely lacking in *Aptenodytes*. Unlike *Spheniscus*, there is no continuous cavity in cross-section; instead, a trabecular network extends across the entire area and divides it into numerous small cavities (a medulla rather than medullary cavity: Fig. 4, top cross-section). The long axes of these trabeculae are oriented at a slight angle to the cranial-caudal plane. The transition from the medulla to the cortex is not discrete. Instead, a transitional region of compacted coarse cancellous bone occurs between the medulla and the denser outer cortex. In this region, woven-fibered struts are secondarily compacted with parallel-fibered bone, giving this region a 'folded' appearance (Fig. 4c), similar to that described by Enlow (1962) in compacted coarse cancellous bone tissue (e.g. fig. 22 in that reference). Within the cortex proper, the compact bone has a more typical appearance. Primary tissues are composed of woven bone well vascularized by reticular primary vascular canals over much of the section. Substantial remodeling is visible throughout the section, with dense occurrences of secondary osteons identifiable by cement lines (Fig. 4a). A particularly large longitudinal vascular canal passes through the cortex on the ventral side (Fig. 4, top cross-section); this is a passageway for the blood vessels entering the bone at the nutrient foramen. The zone of centripetal lamellae surrounding the nutrient canal has a 'smeared' appearance,

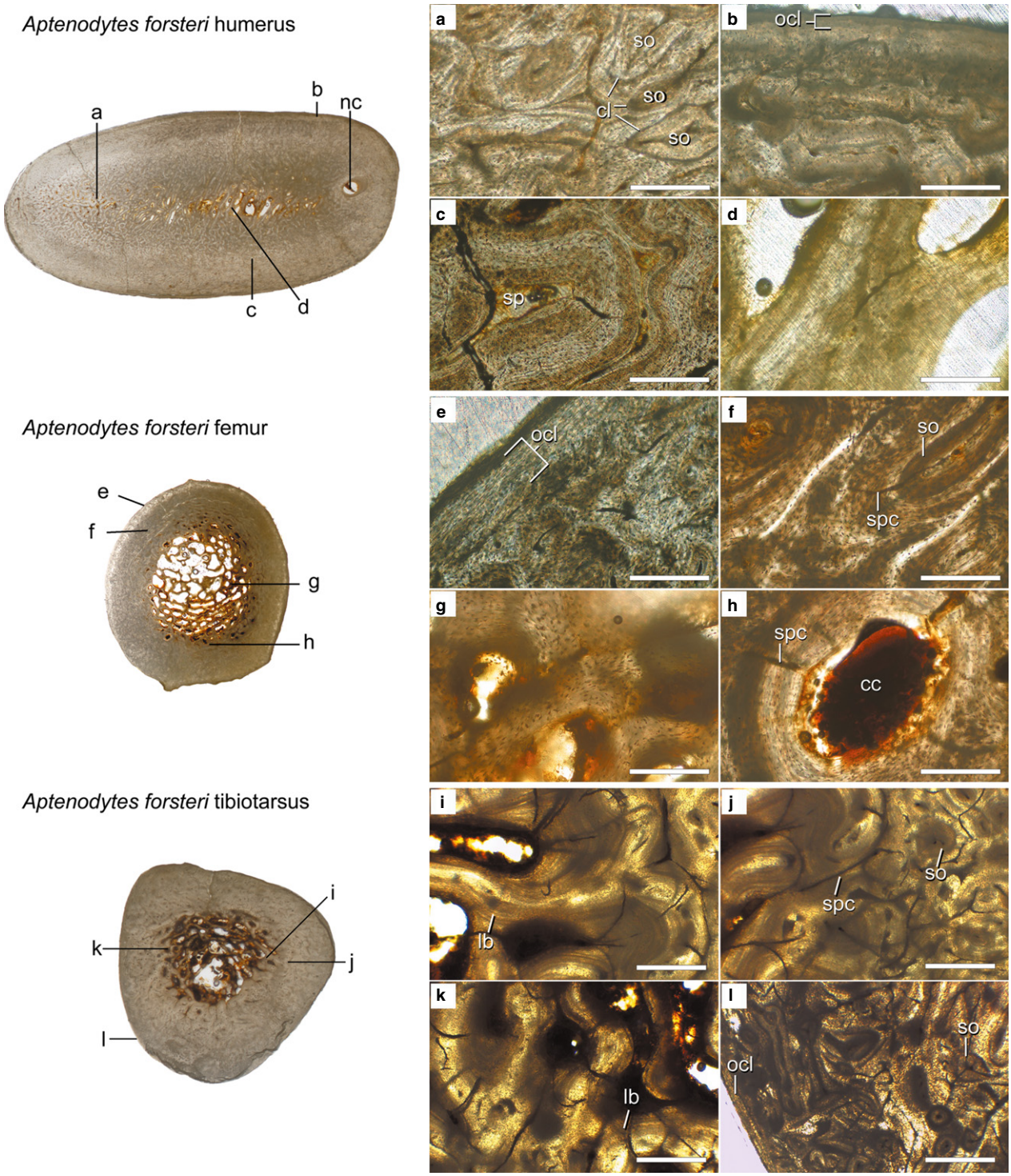

Fig. 4 Histological cross-sections from the mid-diaphyses of *Aptenodytes forsteri* (AMNH 3728) limb elements. Scanned images of the entire sections (not to scale) are shown at the left and microscope images of key regions of the sections are shown at the right (a–l). Cross-section scans are orientated so that the caudal surface of the humerus and the cranial surfaces of the femur and tibiotarsus face the top of the page. Scale bars: 250 μm (a–h); 500 μm (i–l). Abbreviations: cc, central canal; cl, cement line; lb, lamellar bone; nc, nutrient canal; ocl, outer circumferential layer; so, secondary osteon; sp, spaces within folded bone; spc, simple primary canal.

indicating the canal traveled at a relatively high angle to the long axis of the bone. A thin OCL of parallel-fibered bone is present (Fig. 4b).

Compared with *Spheniscus*, the femur of *Aptenodytes forsteri* has an unusually thin cortex and a larger medullary cavity that is mostly filled by thin trabeculae (Fig. 4, middle cross-section). The

interstitial spaces between these are large, consistent with previous reports for this species (Chinsamy et al. 1998). The trabeculae are composed of woven-fibered bone and are not generally lined by lamellae (Fig. 4g). The transition to the cortex is abrupt. In the innermost cortex, a thin band of erosion rooms is visible. These are lined by parallel-fibered bone rather than lamellae, and short simple primary canals extend radially from the central canal to the border of the parallel-fibered bone (Fig. 4h). In the midcortex, primary bone tissues are woven-fibered and moderately vascularized by short circumferential or reticular simple primary canals (Fig. 4f). Secondary osteons are present throughout the cortex. Near the periosteal surface, there is a thin OCL of avascular, parallel-fibered bone (Fig. 4e). The femoral OCL has a much higher osteocyte density compared with that of the humerus in this individual. Both Meister (1962) and Chinsamy et al. (1998) described a thicker cortex in *Aptenodytes forsteri* femoral sections than observed here.

It is unlikely that AMNH 3728 is a juvenile, as the length of the limb bones fall comfortably within those measured for adult birds of *Aptenodytes forsteri*, and the complete skeleton shows no poorly ossified regions or porous surface texture suggestive of a young animal. Additionally, the femur and humerus each show a well-developed OCL, suggesting that maximum circumference had been attained at the time of death. The full skeleton of AMNH SKEL 3728 exhibits no evidence of lesions, malformation, injury or arthritic bone. However, disease does not necessarily leave identifiable marks on the external surface of the skeleton, so the possibility that the femoral bone structure was modified by sickness or malnutrition remains. Notably, the other bones sampled from this individual appear normal in context of the accounts of Meister (1962) and Chinsamy et al. (1998). In the absence of ontogenetic or pathological difference, it is suggested that cortical thickness is individually variable in the femur of *Aptenodytes forsteri*. In agreement with this inference, a high degree of variation is also observed in the size of the medullary cavity and the degree of development of trabeculae within the medullary cavity in femora of *Pygoscelis antarcticus* based on comparisons between individuals sampled by Wilson & Chin (2014) (UNCW 963 images from Morphobank Project 1270; and UNCW 979 images provided by L. Wilson) and individuals of *Aptenodytes patagonicus* sampled by Canoville (2010: 253).

In the tibiotarsus, the medullary cavity lies off-center and is irregular in shape. In contrast to the *Spheniscus* section, long trabeculae span much of the medullary cavity (Fig. 4, bottom cross-section). These are composed primarily of lamellar bone (Fig. 4i). Most of the perimeter of the medullary cavity is comprised of lamellar or parallel-fibered bone with a wavy appearance (Fig. 4k, left side of Fig. 4j). The transition from cancellous to compact bone is similar to that of the femur. The primary cortex is composed of woven-fibered tissue densely vascularized by large, reticular simple primary canals (Fig. 4j). Secondary osteons are scattered throughout the cortex (Fig. 4j,l), but are particularly numerous in the outer cortex (Fig. 4l). A thin, avascular OCL of parallel-fibered bone is present at the periosteal surface (Fig. 4l).

†*Palaeospheniscus patagonicus*

†*Palaeospheniscus patagonicus*, although occupying a stem position in the penguin phylogenetic tree, exhibits bone microstructure very similar to that of the extant penguins described above. In the humerus, the cortex is thick, with a small and highly flattened medullary cavity (Fig. 5, top cross-section), similar to that of *Spheniscus*. Three wide trabeculae traverse the medullary cavity, but it is largely open. A thin layer of centripetal parallel-fibered bone visible along parts of the cavity's margin indicates minor endosteal bone formation (an ICL; Fig. 5a). Cross-cutting at this abrupt transition to the cortex indicates that the ICL was deposited later and partially replaced some of the cortical bone, a process known as cortical drift. Such a change may reflect responses to changing stresses in the bone or regional shifts in the rate of growth (de Margerie, 2006). The inner cortex (Fig. 5c) and midcortex (Fig. 5b) are composed of woven-fibered bone tissue well vascularized by reticular canals (both simple primary canals and primary osteons) of irregular lengths. There are more radially oriented vascular canals along the cranial face of the bone. In the region immediately internal to the periosteal surface, osteons are small and the vascular canals are primarily longitudinally oriented (Fig. 5d). Dark staining has obscured the outermost layer of the humerus. Nowhere is a clearly defined OCL visible, but it is likely the layer was lost to wear given that the fossil was collected in isolation and in damaged condition.

The femur of †*Palaeospheniscus patagonicus* is similar to that of *Spheniscus* in its gross morphology, but differs in its microstructure. The medullary cavity, which is partially infilled with dark minerals, is larger than that of *Spheniscus* both absolutely and relative to the cross-sectional area; it is more similar to that of *Aptenodytes* in its proportions (Fig. 5, middle cross-section). The few trabeculae present are unusually oriented; they run parallel to the endosteal margin rather than extending inwards from it (Fig. 5f). It may be that these are pieces of the cortex that detached from the endosteal margin and were moved inwards post-fossilization, but this is unlikely. In several places along the endosteal margin, the bases of these centripetal trabeculae are still confluent with the cortical tissues. In these cases, it is apparent that they make a 90° turn in orientation immediately upon entering the medullary cavity. In other places, it is clear from focusing through the plane of section that the trabeculae have a broad, shelf-like attachment to the cortex more proximally or distally (Fig. 5f). This unusual morphology may result from resorption occurring circumferentially along the endosteal margin rather than in the more typical oval or circular shapes.

The innermost cortex of the femur is largely composed of compacted coarse cancellous bone (Fig. 5f), with bands of parallel-fibered bone compacting thick cores of woven-fibered bone. The rest of the cortex is composed of primary woven-fibered bone tissue, but vascularization varies around the section. In most regions, the primary osteons are large, vascularization is dense and canals are irregularly arranged (Fig. 5e). In one region, the canals show a strong radial pattern (Fig. 5h). Near the periosteal surface of the bone, osteons are smaller and shorter, with fewer anastomoses, and thus vascularization is poor (Fig. 5g). As in the humerus, dark staining obscures the outermost tissues and the periosteal surface.

The tibiotarsus section of †*Palaeospheniscus patagonicus* is dissimilar to those of the extant taxa at the macro- and microstructural scales, though this is likely due in part to the more distal level of sampling (Fig. 2). The bone has a very thick cortex with a small oval medullary cavity. It differs from *Aptenodytes* in lacking trabeculae (Fig. 5, bottom cross-section), but this may be preservational or represent variation along the length of the shaft. The endosteal margin preserves a very thin ICL of lamellar and parallel-fibered bone in a few places (Fig. 5l). Based on the orientation of lamellae and osteocytes, the ICL clearly has been eroded, but it is impossible to determine whether this occurred during life or during mineral infilling. Several osteons have been truncated at the medullary cav-

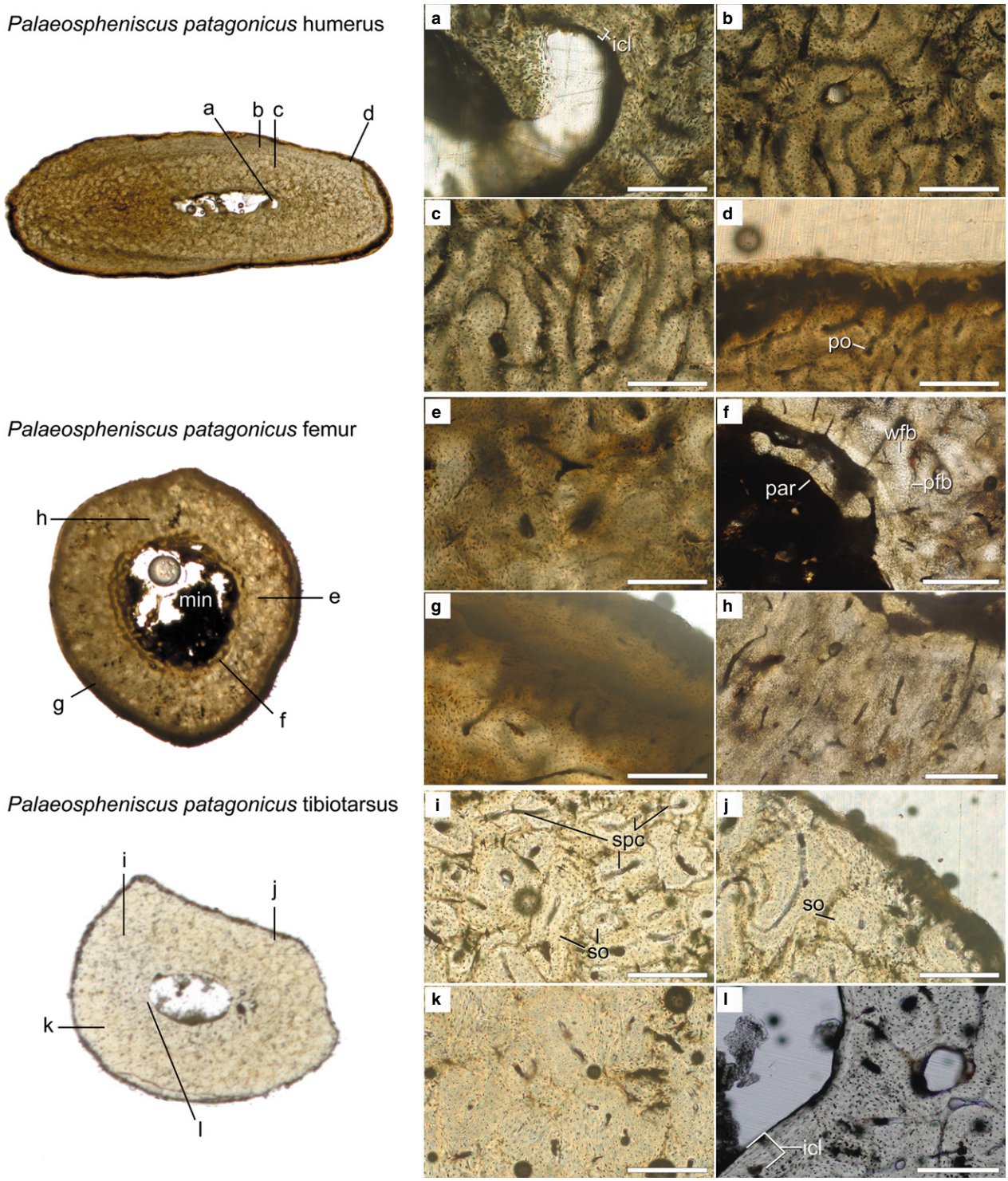

Fig. 5 Histological cross-sections from †*Palaeospheniscus patagonicus* humerus (AMNH FARB 3287), femur (AMNH FARB 3349) and tibiotarsus (AMNH FARB 3321). Sections are taken from the mid-diaphyses except in the tibiotarsus (distal diaphysis). Elements are not likely from the same individual. Scanned images of the entire sections (not to scale) are shown at the left and microscope images of key regions of the sections are shown at the right (a–l). Cross-section scans are orientated so that the caudal surface of the humerus and the cranial surfaces of the femur and tibiotarsus face the top of the page. Scale bars: 250 μm (a–e, g, i–l); 500 μm (f, h). Abbreviations: icl, inner circumferential layer; min, mineral deposits; par, parallel trabecula; pfb, parallel-fibered bone; po, primary osteon; so, secondary osteon; spc, simple primary canal; wfb, woven-fibered bone.

ity boundary, suggesting osteoclastic activity removed preexisting bone to create the smooth medullary cavity border. Secondary remodeling is pervasive throughout the cortex. Densely packed secondary osteons cut across primary osteons and other secondary osteons, and very little of the primary tissues remain (Fig. 5i,j). The secondary osteons anastomose with each other in all directions via simple canals, which are regionally abundant (Fig. 5i). No OCL is preserved, as the periosteal surface was abraded from weathering or during preparation (Fig. 5j).

†Small Eocene stem penguins

The small Eocene fossil humerus examined here differs dramatically from extant penguins in possessing a much larger medullary cavity (Fig. 6, top cross-section). A few trabeculae cross the edges of the central space, but this region is otherwise open (although, note that some dark mineral deposits have formed within the fossil). The boundary between the medullary cavity and cortex is sharply defined in some areas, but poorly delineated in others. At the ventral edge, there is an abrupt transition from the open medullary cavity to the cortex, despite the lack of an ICL. In contrast, along the transect from medullary cavity to the dorsal periphery of the bone the medullary cavity becomes more densely occupied by trabeculae, grading into an area of loosely compacted cortex with numerous open spaces that decrease in size and abundance periosteally (Fig. 6b). These trabeculae each have a core of primary, woven-fibered tissue that was subsequently compacted with parallel-fibered bone (Fig. 6a), similar to the inner cortex of the humerus of *Aptenodytes* and the femur of †*Palaeospheniscus*. The inner two-thirds of the humeral cortex is almost entirely composed of primary woven-fibered and parallel-fibered tissue; thin strips midway between canals are woven-fibered, which grades into parallel-fibered bone approaching the primary osteons (Fig. 6c). The proportion of woven-fibered to parallel-fibered tissue varies around the circumference of the section.

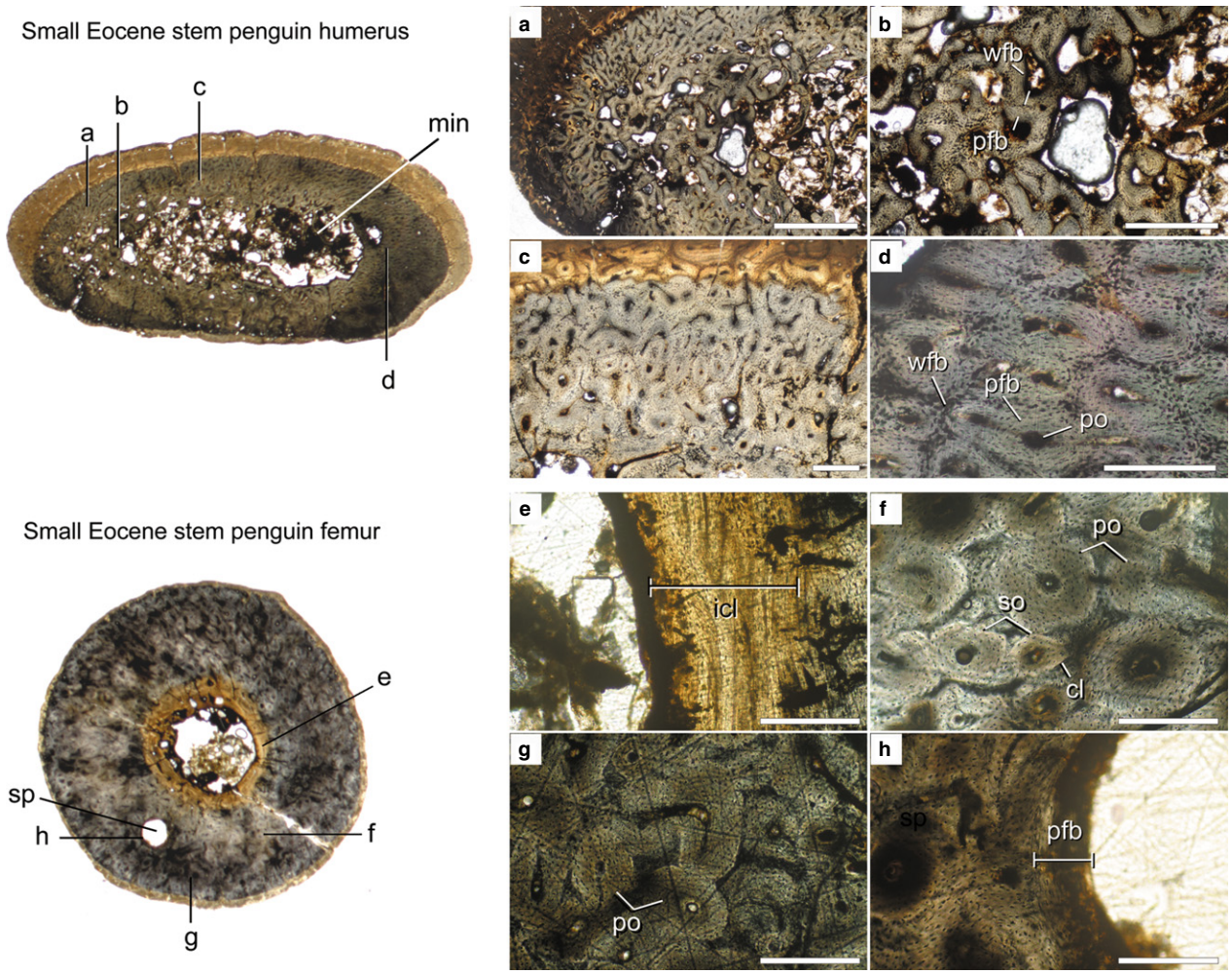

Fig. 6 Histological cross-sections from the mid-diaphyses of small Eocene stem penguin humerus (USNM 404461) and femur (USNM 404459). Elements are not likely from the same individual. Scanned images of the entire sections (not to scale) are shown at the left and microscope images of key regions of the sections are shown at the right (a–h). Cross-section scans are orientated so that the caudal surface of the humerus and the cranial surface of the femur face the top of the page. Scale bars: 500 μm (a, d); 1 mm (b); 250 μm (c, e–h). Images (a–d) mirrored horizontally and images (e–h) mirrored vertically to aid comparison with other figures. Abbreviations: cl, cement line; icl, inner circumferential layer; min, mineral deposits; pfb, parallel-fibered bone; po, primary osteon; so, secondary osteon; sp, open space in cortex; wfb, woven-fibered bone.

Within the cortex, there is a great deal of variation in the vascular structures in different regions of the section. Near the cranial and caudal borders of the medullary cavity, the cortex is composed of very large primary osteons, while smaller osteons form the cortex adjacent to the endosteal margin. Orientation of the vascular canals also varies across the section. The general pattern consists of predominately longitudinal canals at the deepest part of the cortex, transitioning to reticular or radially oriented canals closer to the periphery, and shifting back to a longitudinal pattern at the periphery (a transitional zone visible in Fig. 6c). In this specimen, a deep zone of staining occurs near the periosteal surface, particularly along the caudal surface. Primary osteons persist to the outermost preserved edge of the bone. These osteons are often compacted with lamellar bone and separated by interstitial parallel-fibered tissue, suggesting slower growth than for the inner cortex. However, there is no OCL observable. In some regions, the periosteal margin shows clear signs of abrasion. Given that the outer cortex shows histological signs of slowed growth, the possibility that a thin OCL was originally present and subsequently lost to abrasion should be considered.

As in †*Palaeospheniscus*, the small Eocene stem penguin femur does not likely represent the same individual as the humerus, although both elements are likely from adults based on size and surface texture. The femur is circular in cross-section, with a circular, open medullary cavity that lies centrally (Fig. 6, bottom cross-section). Cortical thickness is slightly higher than that of the *Spheniscus* femur, contrasting with the less compact humerus.

As in the humerus, the femoral medullary cavity is partially infilled by dark matrix and calcite crystals. The ICL is stained brown, and is composed of lamellar bone that regionally grades into parallel-fibered bone. It is occasionally crossed by radial primary osteons or simple primary canals. The ICL forms a complete ring and is quite thick compared with other penguins surveyed (Fig. 6e). Very few trabeculae extend into the medullary cavity, although it is possible some were lost to mineral invasion post-depositionally; small bits of lamellar and parallel-fibered bone are present within the matrix infill.

Most of the cranial half of the cortex is vascularized by longitudinal secondary osteons. These are generally lined with parallel-fibered bone, but some show a few distinct lamellae close to the vascular space. In some regions of the bone, several generations of secondary osteons cut across each other, whereas in others, small patches of the original woven-fibered primary tissues are visible between osteons. In the caudal half of the section, the canals are primary osteons lined by parallel-fibered tissue. As in *Spheniscus*, their orientation is predominately longitudinal (Fig. 6g), though radially oriented canals proliferate in one sector, near to the linea intermuscularis cranialis. A large, circular open space is visible at midcortex in this section (Fig. 6, lower cross-section), but it does not appear in more distal sections of this bone (not shown). Centripetal deposits of parallel-fibered bone around the periphery of this opening (Fig. 6h) indicate the space is not an artifact of damage. It is possible this structure represents a localized resorption zone, or it may be an unusually large vascular canal for the vessels entering at the nutrient foramina. In this quadrant of the bone, some small secondary osteons with distinct cement lines are visible (Fig. 6f).

The external-most cortex of the femur is also stained a brownish color but, unlike the ICL, it has a dull appearance. This staining obscures most of the microstructure of the outermost layer of bone, but in some regions it is possible to discern that primary and secondary osteons persist to the outer edge of the bone. No OCL is observable but, as discussed above, this does not necessarily indicate absence. Because some of the secondary osteons at the bone's surface are truncated externally, an OCL would have been destroyed by wear if it were present.

†Large Eocene stem penguins

As in all other taxa, the humerus of the large Eocene stem penguin is oval in cross-section (Fig. 7, top cross-section). The unusually small, round medullary cavity is not located in the center of the shaft, but is instead displaced ventrally. The medullary cavity is mostly open and has a distinctly circular shape, contrasting strongly with the compressed, slit-like medullary cavity of extant penguins. Along much of its margin, the medullary cavity is surrounded by a rather thick ICL, which is composed of parallel-fibered bone and well-vascularized by radial simple primary canals (Fig. 7b). However, the endosteal margin is not completely smooth and irregularly shaped bridges of bone encroach upon the medullary cavity. Whether or not bone was actively being deposited along the ICL at the time of death, it is clear from the thickness of the ICL that medullary cavity expansion had ceased.

External to the ICL, the structure of the mid-diaphyseal cortex is quite variable in different regions around its circumference. In the inner third of the cortex, bone porosity reaches as high as 50% (Fig. 7, top cross-section; Fig. 7d). Porosity is also high in the outer cortex of the medial and lateral quadrants. In these porous regions, the struts of bone are composed of woven-fibered bone and may bear primary osteons. Osteocyte density is highest at the center of the struts. In some regions, the struts are lined with weakly woven bone or parallel-fibered bone. The spaces between struts are irregularly shaped. The microstructure of these porous regions suggests rapid peripheral expansion occurred, with the pace of periosteal expansion exceeding the ability of the primary osteons to complete bone formation.

The densest (most compact) regions of the bone occur near the periphery, particularly in the unstained (gray) regions along the cranial and caudal faces of the bone. Many longitudinal primary osteons are present in the compact regions. These frequently anastomose, and the arrangement of the anastomoses varies from oblique to irregularly branching (subreticular) patterns (Fig. 7a). As in the porous regions, central cores of woven-fibered bone are present in the interstices between canals, and the canals are compacted by parallel-fibered bone. However, the woven component of the bone is proportionately much smaller compared with the deeper cortex (Fig. 7c). Infilling of the vascular canals is complete in these regions and the bone is largely primary in origin, with little evidence of secondary remodeling. Close to the periosteal surface, the tissue is stained a darker brown and is composed entirely of compact parallel-fibered bone. This region is vascularized by longitudinal primary osteons and simple canals arranged in circumferential rows. These canals do not form extensive anastomoses and are smaller in diameter compared with more internal tissues. There is no OCL, although as noted for the other Eocene penguins, abrasion of the surface may have removed the outermost growth record.

The much higher density of the outer cortex compared with the internal regions is consistent with the endosteal trajectory of compaction (Enlow, 1962), but it has not occurred to the extent observed in the *Aptenodytes* and †*Palaeospheniscus* humeri described above. This may reflect ontogenetic differences between individuals. However, the decreased canal diameter, vascular pattern and extent of anastomoses, and the transition to

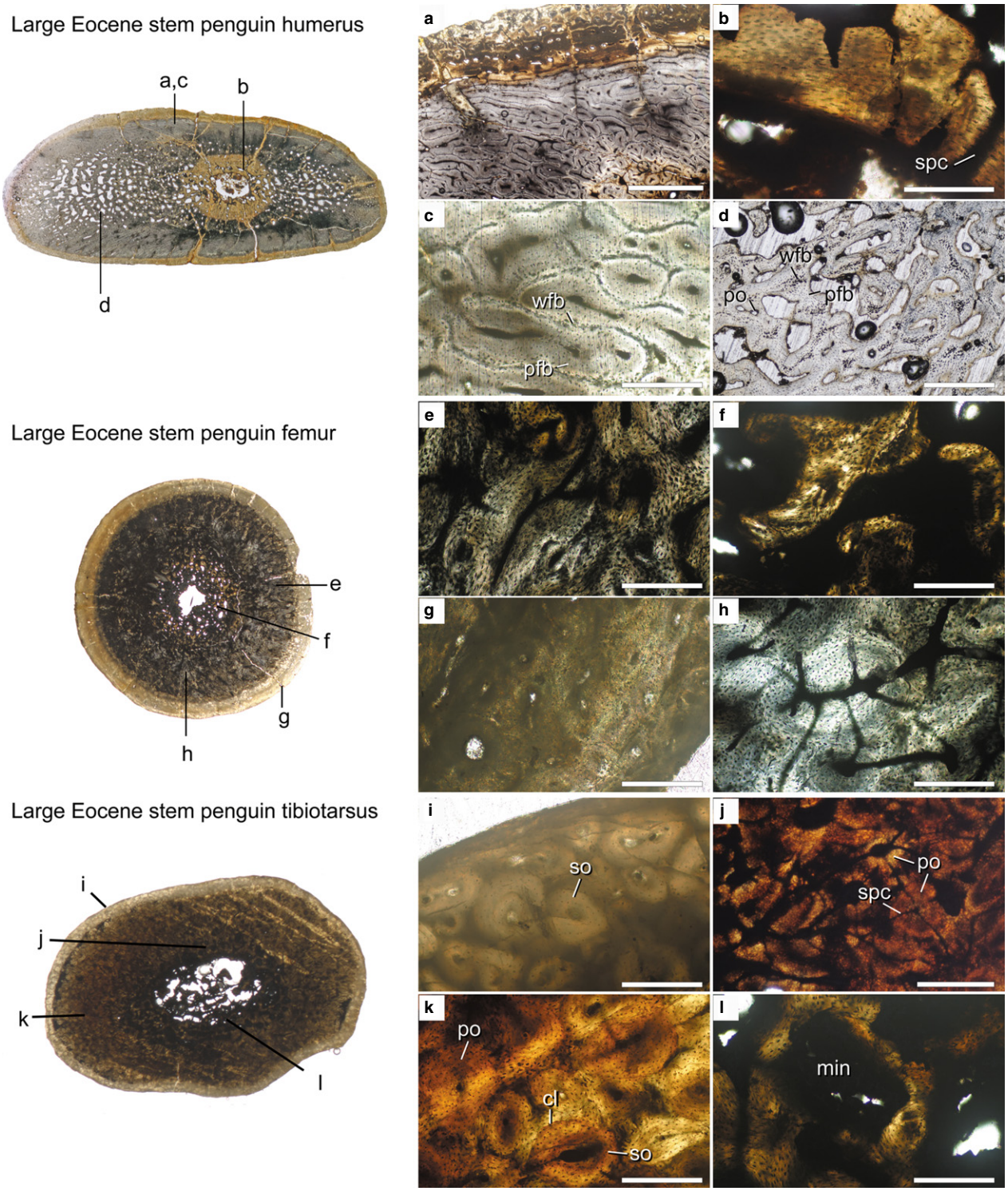

Fig. 7 Histological cross-sections from the mid-diaphyses of large Eocene stem penguin humerus (USNM 404477), femur (USNM 402616) and tibiotarsus (USNM 402351). Elements are not likely from the same individual. Scanned images of the entire sections (not to scale) are shown at the left, and microscope images of key regions of the sections are shown at the right (a–l). Cross-section scans are orientated so that the caudal surface of the humerus and the cranial surfaces of the femur face the top of the page. Images (a–d) mirrored horizontally to aid comparison with other figures. Scale bars: 1 mm (a); 250 μm (b–i, k, l); 500 μm (j). Abbreviations: cl, cement line; min, mineral deposit; pfb, parallel-fibered bone; po, primary osteon; so, secondary osteon; spc, simple primary canal; wfb, woven-fibered bone.

parallel-fibered bone in the outermost cortex suggest that this individual was close to or had reached adult size at time of death.

As in the other fossil taxa, the femur is likely from a different individual than the humerus. It is circular in cross-section, with a thick cortex and small medullary cavity that sits centrally (Fig. 7, middle cross-section). The most distinguishing feature of the large Eocene penguin femur is the unique structure of the medullary cavity and surrounding tissues. Unlike the other femora surveyed, the boundary of the medullary cavity is not well-defined. Instead, there is a thick layer of cancellous primary bone surrounding a small, irregularly shaped medullary cavity. The bone tissue here is darkly stained but, where visible, the osteocytes appear disorganized, suggesting woven-fibered bone (Fig. 7f). Near the endosteal margin, the primary osteons have a highly disorganized, reticulate orientation and are of moderate size (Fig. 7e). A clear transition in canal appearance occurs along the radial transect from the endosteal margin to the periosteal margin. In a thick section near the outer periphery, canal orientation becomes primarily longitudinal, and the primary osteons become much smaller (Fig. 7g,h). Vascularization remains dense throughout the cortex. Unlike the humerus, the bone is almost entirely composed of woven-fibered tissues; the canals are lined with but not significantly compacted by parallel-fibered bone. No OCL is observed in the large Eocene femur but, as mentioned above for the small Eocene penguin, this may be the result of wear.

In cross-section, the tibiotarsus has a more flattened (oval) shape than the extant taxa. The shape of the central medullary cavity is slightly irregular, but roughly parallels the external borders of the cross-section (Fig. 7, bottom cross-section). The medullary cavity is partially invaded by trabeculae, and is surrounded by a region of cancellous parallel-fibered and lamellar bone (Fig. 7l). Almost all of these spaces as well as parts of the medullary cavity are infilled with an opaque dark gray mineral. The innermost cortex is densely vascularized by large, longitudinal primary osteons. Each of these anastomose with adjacent osteons in many directions by short primary canals, forming reticulations (Fig. 7j). Moving periosteally, the primary osteons decrease in diameter, and anastomose less frequently (Fig. 7k). Haversian remodeling is common throughout the cortex, but the interstices between secondary osteons show patches of the original woven-fibered bone tissue. A conclusive OCL is not visible at this bone's periphery (Fig. 7i), though staining, remodeling and wear obscure the primary tissues of the external-most cortex around most of the circumference.

Compactness and CDI

The relative compactness of the long bone cross-sections used for Bone Profiler data collection is illustrated in Fig. 8. CDI and compactness values are reported in Table 2.

Compactness and CDI values in all penguin taxa were higher than those in outgroup taxa for each of the three sampled elements (Table 2). However, different elements exhibited different patterns. Notably, the small Eocene penguin exhibited a humeral compactness value only slightly higher than the outgroup loon, whereas the remaining four penguin taxa exhibited substantially higher values. The difference between the small Eocene penguin and the remaining taxa is even larger for CDI values, which also show more variation between the two crown penguins. It is important to note that the large Eocene penguin achieves high compactness and CDI values through a combination of a small, circular medullary cavity and 'spongy' compacta. That is, despite the less solid compacta, the marrow cavity is smaller in area compared with flattened, dorsoventrally elongated medullary cavity of †*Palaeospheniscus patagonicus* and the extant penguins. In contrast to the humerus, there is less variation in hind limb element compactness and CDI values across sampled penguins. The small Eocene penguin and large Eocene penguin actually exhibit slightly higher compactness values and substantially higher CDI values than the extant penguins. Finally, it is interesting to note that the humerus CDI and compactness values exceed the hind limb bone values in both outgroup taxa, including the foot-propelled diving Common Loon (*Gavia immer*).

Discussion

Osteosclerotic bone structure can develop via multiple pathways (de Ricqlès & de Buffrénil, 2001). One mechanism is the inhibition of chondroclastic and/or osteoclastic activity. Slowing the rate of expansion of the medullary cavity relative to overall bone circumference growth rate will result in a smaller medullary cavity and thicker cortex at completion of growth. A second mechanism is endosteal filling, which will secondarily reduce the size of the medullary cavity. A third mechanism is replacement of cancellous bone with compact bone, either by Haversian remodeling (de Ricqlès & de Buffrénil, 2001) or delayed compaction of canals by additional primary tissues (Enlow, 1962). Combinations of these processes can also occur in the same organism.

In order to fully understand both the ontogeny and evolution of bone microstructure in penguins, ontogenetic series are desirable. Such data are not yet available for any fossil penguin taxon. However, substantial information is available for extant penguins and provides a starting point for reconstructing an ontogenetic framework within which to consider patterns in fossil taxa. Histological studies have demonstrated that penguin hatchlings exhibit cancellous bone cortices and possess a relatively large medullary cavity partially occupied by trabeculae (de Margerie et al. 2004). This conformation is the result of rapid expansion of the periosteum exceeding the primary osteon filling process (de Margerie et al. 2004). Later in ontogeny, additional periosteal deposition at the surface of the cortex, infilling of the marrow cavity via endosteal deposition, and infilling of secondary osteons contribute to the high level of compactness in adult bones (Canoville, 2010: fig. 9). Although the cortex is thin in extant penguin chicks compared with adults, it should be noted that it is still relatively thicker than in the adults of most living birds, indicating that the expansion of the medullary cavity is delayed relative to bone circumference growth in living penguins. Ontogenetic data from extant penguins are thus consistent with a model in which both the inhibition of perimedullary resorption and the compaction of cancellous tissues play an important role in the development of osteosclerosis.

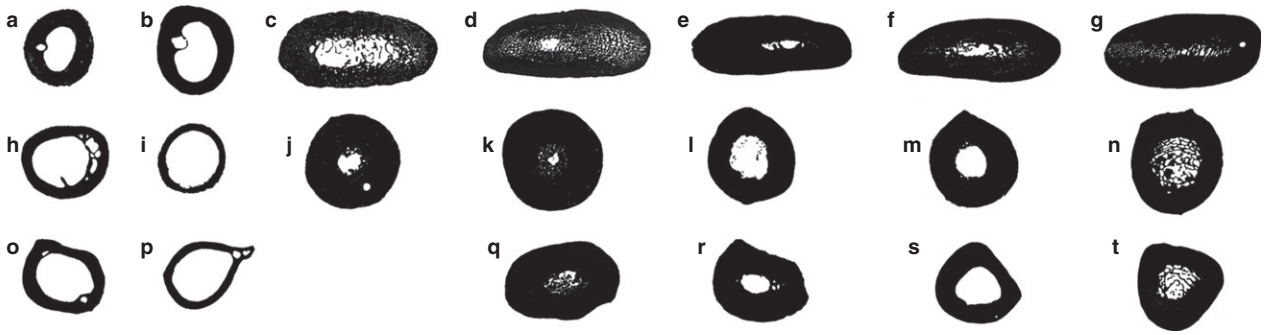

Fig. 8 Black and white images of long bone cross-sections used for Bone Profiler data collection, showing the relative compactness of penguins and outgroup taxa. Humerus of (a) *Gavia immer*, (b) *Calonectris borealis*, (c) †small Eocene stem penguin, (d) †large Eocene stem penguin, (e) †*Palaeospheniscus patagonicus*, (f) *Spheniscus* sp. and (g) *Aptenodytes forsteri*. Femur of (h) *Gavia immer*, (i) *Calonectris borealis*, (j) †small Eocene stem penguin, (k) †large Eocene stem penguin, (l) †*Palaeospheniscus patagonicus*, (m) *Spheniscus* sp. and (n) *Aptenodytes forsteri*. Tibiotarsus of (o) *Gavia immer*, (p) *Calonectris borealis*, (q) †large Eocene stem penguin, (r) †*Palaeospheniscus patagonicus*, (s) *Spheniscus* sp. and (t) *Aptenodytes forsteri*. See Table 1 for specimen numbers. Images not to scale.

Table 2 Compactness and CDI values estimated for sampled specimens, with additional *Pygoscelis* values based on images from Wilson & Chin (2014).

Specimen	Compactness	CDI
Gavia immer humerus	0.726	0.485
Calonectris borealis humerus	0.636	0.395
†Small Eocene humerus	0.775	0.535
†Large Eocene humerus	0.897	0.850
†*Palaeospheniscus* sp. humerus	0.875	1.123
Spheniscus sp. humerus	0.879	0.828
Aptenodytes forsteri humerus	0.917	1.374
Gavia immer femur	0.524	0.319
Calonectris borealis femur	0.370	0.207
†Small Eocene femur	0.941	0.778
†Large Eocene femur	0.984	0.947
†*Palaeospheniscus* sp. femur	0.805	0.555
Spheniscus sp. femur	0.877	0.654
Aptenodytes forsteri femur	0.884	0.520
Pygoscelis antarcticus femur (UNCW B979)	0.820	0.700
Pygoscelis papua femur (UNCW B980)	0.872	0.639
Gavia immer tibiotarsus	0.549	0.333
Calonectris borealis tibiotarsus	0.411	0.234
†large Eocene tibiotarsus	0.974	0.758
†*Palaeospheniscus* sp. tibiotarsus	0.922	0.727
Spheniscus sp. tibiotarsus	0.743	0.498
Aptenodytes forsteri tibiotarsus	0.891	0.616
Pygoscelis antarcticus tibiotarsus (UNCW B979)	0.885	0.687
Pygoscelis papua tibiotarsus (UNCW B980)	0.872	0.639

CDI, cortico-diaphyseal index.

Growth patterns in extinct penguins

Determining the general growth patterns in 'giant' fossil penguins is one key to understanding the paleobiology of these enigmatic taxa. As mentioned above, the lack of growth series for extinct species limits our ability to reconstruct these patterns. Likewise, precise age cannot be observed for the individuals represented by sampled fossils. This requires that an additional degree of uncertainty be acknowledged for all interpretations.

As noted above, the Seymour Island fossils appear to belong to adult individuals based on size (though note extant penguins reach adult bone lengths before sexual maturity; Canoville, 2010), proportions, and development of features such as muscle insertion scars and surface texture. Nonetheless, the lack of an intact OCL leaves us without definitive evidence of adult status. With a few rare exceptions, Seymour Island penguin fossils are recovered as disarticulated (commonly isolated) elements with heavy abrasion, and the authors therefore believe it is most likely the OCL was lost to weathering. This is in congruence with the observations of Cerda et al. (2015), who reported an OCL in one specimen of *Delphinornis larseni* but found no evidence of an OCL in eight other Seymour Island penguin tarsometatarsi, which they considered to represent adults (see also Yury-Yáñez et al. 2012). Fortunately, this issue has the potential to be resolved by sectioning specimens preserving an intact OCL should such fossils be identified. However, due to the reluctance of institutions to permit destructive sampling of well-preserved accessioned specimens, more fieldwork may be needed to accomplish this test.

Despite these uncertainties, histological data from the specimens examined here provide the basis for an initial outline of growth patterns in 'giant' penguins. It has already been established that extant King Penguins have the ability to lay down cortical LAGs (Castanet, 2006). These are not associated with annual pauses in growth as in most tetrapods that form LAGs, but instead with a fasting period during early growth. No cortical LAGs were deciphered in any of the fossils sampled in this study (although one LAG

was observed within the OCL of the extant *Spheniscus* femur). Thus, as far as can be determined, growth appears to have been relatively continuous from hatching to adulthood in all of the sampled fossil taxa. The absence of LAGs in fossil material suggests that despite their enormous size, giant penguins grew to adult body size without a major pause in bone deposition, which likewise implies they did not undergo a prolonged fasting interval prior to concluding skeletal growth. This observation holds true regardless of whether or not the individuals sampled had reached breeding age, as they had attained adult bone dimensions.

Although the absence of LAGs precludes constructing growth curves for extinct penguins, qualitative features also support the inference of rapid growth rates. In all specimens examined, the primary tissues comprising the bulk of the cortex were either exclusively woven-fibered or contained a substantial woven-fibered component. Studies of mammals and birds have established that in primary bone tissue, woven-fibered bone is deposited at faster rates than parallel-fibered or lamellar bone (Newell-Morris & Sirianni, 1982; de Buffrénil & Pascal, 1984; Castanet et al. 2000; de Margerie et al. 2002). Additionally, all bones that preserved primary vasculature were also very well vascularized and often showed extensive anastomoses. It has long been recognized that animals with high levels of long bone vascularity also have higher growth rates (Amprino, 1947; de Ricqlès, 1975; Francillon-Vieillot et al. 1990), and this has recently been shown empirically across amniotes, including birds (Montes et al. 2010; Cubo et al. 2012).

Blood vessel canal orientation in primary bone tissue may provide additional information on growth rate (Amprino, 1947; de Ricqlès, 1975; Francillon-Vieillot et al. 1990; Castanet et al. 2000). However, it has also been shown that extrapolating a numeric growth rate from bone tissue type alone is not plausible due to large overlaps in growth rates recorded during the deposition of different types of bone (Castanet et al. 2000; de Margerie et al. 2002, 2004). Thus, the most that can be said from the data at hand is that the prevalence of woven-fibered bone, well-vascularized bone tissue and the reticular patterning of vascular canals exhibited by fossil penguins is consistent with very high rates of growth in both small and giant fossil taxa, but absolute values cannot be placed on these rates.

Evolution of osteosclerosis in penguins

The humeri of the Eocene stem penguins are much more cancellous compared with extant forms, whereas the femora and tibiotarsi are more compact. There are two plausible explanations for the differences in humeral microstructure between the Eocene and extant penguins: these features may be plesiomorphic or they may be related to ontogeny. The authors believe an ontogenetic explanation is unlikely as it would require an unusual taphonomic bias resulting in the preservation of vast numbers of juvenile humeri and adult hind limb elements would have been collected from the same locality. A 'spongy' cross-section is consistently observable in dozens of broken humeri of large penguins from the La Meseta Formation in the collections of the UCMP and USNM (DTK personal observation). Humeri of small taxa that expose the medullary cavity are less common in collections, but the larger medullary cavity reported in the small Eocene specimen described here was noted in one uncataloged UCMP specimen. The authors therefore consider the sampled bones to represent adult individuals pending compelling evidence to the contrary.

On a macroevolutionary scale, it is proposed that two key transitions can be identified in the transition from the typical hollow avian humerus to the dense osteosclerotic humerus in penguins, both of which occurred or at least continued after the loss of aerial flight. The first stage is defined by a clear trend in reduction of the overall size of the medullary cavity. The medullary cavity is large in the most basal taxa sampled (small Eocene stem penguin specimens), but is greatly reduced in all other taxa included in the current study, as indicated by comparisons of CDI values (Table 2). The most likely mechanism for this transition is a progressive decrease in endosteal resorption relative to appositional bone deposition, resulting in a smaller medullary cavity at the cessation of growth.

The second stage is defined by a reduction in the 'sponginess' of the bone. All of the Eocene taxa observed here show highly cancellous bone structure, with abundant open spaces in the humerus. In extant penguins and †*Palaeospheniscus*, such spaces are almost entirely absent. A more compact cortex may have been attained in these advanced taxa through delayed canal-ward compaction and Haversian remodeling. Interspersion of primary osteons within a matrix of irregular, 'wavy' woven-fibered bone in extant penguins suggests open spaces appeared as rapid osteogenesis proceeded outward, and were subsequently filled by slower centripetal deposition of parallel-fibered bone later in ontogeny. In the Eocene penguins, rapid osteogenesis appears to have laid down a cancellous web of fibrous bone over much of the inner portion of the cortex, but the subsequent round of canal-ward compaction observed in extant penguins apparently did not take place in Eocene forms. Thus, open spaces remained in the adult bone. Despite the differences in microstructure, there was actually little difference in compactness values between the large Eocene taxon and the extant penguins (Table 2), because the compact bone immediately surrounding the small round medullary cavity offsets the lower compactness of the cortex.

Moreover, histological investigations of the microstructure of the femur and tibiotarsus do not reveal the same patterns as observed in the humerus. In fact, the compactness and CDI values for the hind limb bones of the Eocene stem taxa were higher than those observed in extant penguins. Rather than retaining a large medullary

cavity, the femora of the Eocene penguins actually show a slight reduction of the medullary cavity size compared with that in extant penguins, though at least the large Eocene stem penguins also exhibit a larger proportion of cancellous bone.

Overall, the current data are consistent with the hypothesis that large shifts in humeral microstructure occurred along an interval of penguin evolutionary history that post-dates the loss of aerial flight. This suggests that penguin humerus structure did not reach the highest levels of compactness immediately, but instead continued to evolve for tens of millions of years after the loss of flight. In contrast, the hind limb elements appear to have attained modern levels of compacta thickness earlier in penguin evolution, though the significance of this remains unclear. Certainly, the structure of the flipper bones may have been subject to different selective pressures than the structure of the hind limb bones given the wing-propelled diving ecology of penguins. Better understanding of these patterns will require additional data from the most basal known penguins, such as *Waimanu manneringi* and *Waimanu tuatahi*.

Comparisons to other diving birds

Sphenisciformes represent one of four avian lineages that independently acquired a flightless wing-propelled diving ecology, the others being the Plotopteridae (an extinct clade of Suliformes), and two flightless lineages of Pan-Alcidae: Mancallinae (extinct stem alcids) and the small group of species related to the Great Auk (†*Pinguinus impennis*). Plotopterids are known to possess dense bone structure (Olson & Hasegawa, 1979). From the available data, Plotopteridae also appear to have evolved an osteosclerotic (as opposed to pachyostotic) bone structure, but the lack of detailed observations on bone microstructure otherwise limits comparisons with penguins. More data are available for Pan-Alcidae following recent histological work by Smith & Clarke (2014), who found that flightless auks exhibit osteosclerotic bone structure in all sampled bones (humerus, ulna and femur).

Pan-alcids provide added insight into evolution of wing-propelled diving, because volant and flightless taxa can be compared. Smith & Clarke (2014) observed that relative bone wall thickness was more than twice as high in the volant wing-propelled diver *Alca* (two species were sampled: *A. torda* and †*A. grandis*) compared with the non-diving outgroup species *Stercorarius longicaudus*. In turn, relative bone wall thickness was > 50% higher in two flightless wing-propelled diving taxa (†*Pinguinus impennis* and †*Mancalla cedrosensis*) than in *Alca*. A similar two-stage pattern of increasing relative bone thickness was observed in the femur of pan-alcids, though bone thickness was much lower for the femur than for the humerus in all sampled taxa, and even the thickness in flightless alcids did not approach values seen in penguins (Smith & Clarke, 2014). Data from Pan-Alcidae are consistent with the hypothesis that both the initial shift to wing-propelled diving and the subsequent loss of flight have a major impact on bone histology. Whether this pattern also occurred in penguins is currently impossible to determine, because volant stem lineage penguins have yet to be discovered. However, further histological explorations within the Procellariiformes, particularly for the wing-propelled diving Pelecanoididae, could help to establish general patterns.

In terms of the cross-sectional properties of the humerus, flightless auks exhibited an overall morphology similar to that of *Spheniscus* and †*Palaeospheniscus*. As in those penguin taxa, the compacta is thick and the ovoid medullary cavity is greatly reduced in size (Smith & Clarke, 2014: fig. 4). In contrast to the penguin taxa, there appear to be no trabeculae entering the medullary cavity in the humeral sections of the two flightless auks (medullary deposits in a Great Auk were identified as medullary bone by Smith & Clarke, 2014), and the medullary cavity is also moderately larger.

At least in the case of the Great Auk lineage, alcids seem to have attained a highly osteosclerotic bone structure in rapid fashion. Divergence dating estimates for the split between †*Pinguinus impennis* and volant auks vary from ~16 Ma (Smith, 2011) to ~24 Ma (Pereira & Baker, 2008), and these dates represent maximum estimates of the amount of time that passed since the loss of flight in the †*Pinguinus* lineage, which may have occurred at any time between this divergence and the age of the oldest †*Pinguinus* fossils at 4.4 Ma (Olson, 1977). This would represent a much shorter span of time than elapsed between the age of the earliest known fossil penguin (the flightless †*Waimanu manneringi* at 60.5–61.6 Ma; Slack et al. 2006) and the age of the most basal penguins studied here (34.7–36.1 Ma). In addition, penguins and pan-alcids appear to display disparate patterns of increasing osteosclerosis throughout the skeleton, as †*Pinguinus* exhibited a relatively thick humerus bone wall and thin femur bone wall (Smith & Clarke, 2014), whereas the most basal penguins sampled here show the opposite pattern.

Constraints on diving bird bone histology

One of the outstanding questions in the evolution of wing-propelled diving birds is why each of the known lineages of pursuit predators converged on an osteosclerotic bone structure, in contrast to the osteoporotic structure seen in most vertebrate diving predators such as marine reptiles and mammals. A general pattern of transition has been recognized in active hunting secondarily marine tetrapods, which includes an initial phase of increased bone density (via osteosclerosis, pachyostosis or pachyosteosclerosis) followed by a transition to secondarily reduced bone density via osteoporosis (Wall, 1983; Taylor, 2000; Houssaye,

2009). Osteoporotic bone microstructure has been observed in cetaceans, ichthyosaurs and mosasaurs, as well as the leatherback sea turtle *Dermochelys coriacea* (Felts & Spurrell, 1965; Rhodin et al. 1981; Rhodin, 1985; de Buffrénil & Mazin, 1990; Sheldon, 1997; Kolb et al. 2011). In contrast, slow-swimming and shallow-diving secondarily marine tetrapods, such as sirenians, sea otters and the extinct Placodontia, tend to maintain high levels of bone density (Domning & de Buffrénil, 1991; de Buffrénil & Mazin, 1992; Taylor, 2000). These taxa are primarily grazers or predators of sessile prey. Penguins and alcids (and presumably plotopterids) clearly fall within the category of active pursuit predators, yet their bone structure more closely resembles that of non-avian taxa that exhibit, or are inferred to have exhibited, a slow-swimming ecology.

The underlying reason for this disparity appears to be linked to physiology. Osteosclerotic bone microstructure can increase density and thus decrease overall buoyancy, which aids in counteracting buoyancy from the lungs and increasing stability (Kaiser, 1966; de Buffrénil & Mazin, 1990; Domning & de Buffrénil, 1991). At the same time, denser bone microstructure increases inertia and thereby limits swimming speed and maneuverability. Thus, Taylor (2000) proposed that bone ballast should not occur in fast-swimming or deep-diving taxa. Such taxa typically exhibit osteoporotic bone microstructure, which is advantageous to rapid acceleration and maneuverability. To compensate for the increased buoyancy, extant animals with osteoporotic bone microstructure are also able to collapse their lungs (Kooyman et al. 1972; Ridgway & Howard, 1979; Falke et al. 1985).

As birds, penguins are unable to collapse their lungs during diving, though they are able to attain impressive dive depth and duration by storing oxygen not only within the respiratory and circulatory systems, but also within the muscles via increased myoglobin concentration and also by utilizing anaerobic metabolism (Kooyman & Ponganis, 1998; Ponganis et al. 2011). Despite the putative disadvantages of being restricted to an osteosclerotic bone microstructure, penguins are accomplished divers and reach depths of up to 564 m with durations of up to 27.6 min (Wienecke et al. 2007; Sato et al. 2010). These values are increasingly impressive when it is taken into consideration that both dive duration and maximum depth are correlated with body size in diving birds (Piatt & Nettleship, 1985; Williams, 1995; Halsey et al. 2006), because the largest extant penguins reach maximum sizes of only ~40 kg (Wilson, 1907; Prévost, 1961; Groscolas, 1986; summarized in Williams, 1995). Notably, some extinct penguins and plotopterids were substantially larger, and overlapped in size with the smallest cetaceans (e.g. the harbour porpoise *Phocoena phocoena*). These taxa may thus have been capable of substantially deeper and/or longer duration dives than living penguins.

Conclusions

Histological investigations reveal a complex pattern of bone microstructure evolution in penguins. Penguins, restricted by their ancestral avian physiology, retained a general osteosclerotic bone microstructure over the entire 60 million year flightless interval of their evolutionary history that has been sampled from the fossil record. However, the evolution of limb bone microstructure does not seem to have been restricted to any single stage of the transition to flightless wing-propelled diving, and these birds continued to modify at least humeral microstructure for a long interval following the initial loss of flight. Furthermore, different limb bones exhibit different levels of osteosclerosis, suggesting that this transition did not occur synchronously throughout the skeleton. Finally, even though the large Eocene stem penguins lack an OCL, the histological transition to slower-growing bone tissue in the outer cortex and the presence of compacted internal tissues suggests they had nearly completed growth. This, coupled with the lack of LAGs in 'giant' penguins, argues against extended pauses during the pre-fledging growth interval in these extinct taxa.

Acknowledgements

The authors thank Mark Norell, Joel Cracraft and Peter Sweet (AMNH), and Storrs Olson and Mark Florence (USNM) for access to specimens and permission to take histology samples, Aurore Canoville (Steinmann Institute, Bonn, Germany) for sharing a copy of her dissertation, Laura Wilson (Sternberg Museum of Natural History) for access to comparative images and Piotr Jadwiszczak, N. Adam Smith, Ignacio Cerda, Holly Woodward, Julia Clarke, and an anonymous reviewer for constructive comments and editing. This work was supported by NSF award DEB 0949899 to D.T.K. and NCSU Office of Undergraduate Research grants to Z.B. and M.S.

References

Amprino R (1947) La structure du tissue osseux envisagée comme expression de différences dans la vitesse de l'accroissement. *Arch Biol* **58**, 315–330.

Amprino R, Godina G (1947) La struttura della ossa nei vertebrate. Ricerche comparative negli amfibi e negli amnioti. *Comment Pont Acad Sci* **11**, 329–467.

Baumel JJ, Witmer LM (1993) Osteologia. In: *Handbook of Avian Anatomy: Nomina Anatomica Avium*, 2nd edn, Vol. 23. (eds Baumel JJ, King AS, Breazile JE, Evans HE, Vanden Berge JC), pp. 45–132. Cambridge, MA: Publications of the Nutall Ornithological Club.

Bourdon E, Castanet J, de Ricqlès A, et al. (2009) Bone growth marks reveal protracted growth in New Zealand kiwi (Aves, Apterygidae). *Biol Lett* **5**, 639–642.

de Buffrénil V, Mazin J-M (1990) Bone histology of the ichthyosaurs: comparative data and functional interpretation. *Paleobiology* **16**, 435–447.

de Buffrénil V, Mazin J-M (1992) Contribution de l'histologie osseuse à l'interprétation paléobiologique du genre *Placodus*. *Rev Paléobiol* **11**, 397–407.

de Buffrénil V, Pascal M (1984) Croissance et morphogénèse postnatales de la mandibule du vison (*Mustela vison* Schreiber): données sur la dynamique et l'interprétation fonctionnelle de dépots osseux mandibulaires. *Can J Zool* **62**, 2026–2037.

Canoville A (2010) Diversité microanatomique et histologique des os longs chez les tétrapodes: inférences paléobiologiques. Doctoral Dissertation, University Pierre et Marie Curie.

Canoville A, Laurin M (2010) Evolution of humeral microanatomy and lifestyle in amniotes, and some comments on palaeobiological inferences. *Biol J Linn Soc* **100**, 384–406.

Castanet J (2006) Time recording in bone microstructures of endothermic animals; functional relationships. *C R Palevol* **5**, 629–636.

Castanet J, Curry Rogers K, Cubo J, et al. (2000) Periosteal bone growth rates in extant ratites (Ostriche and Emu). Implications for assessing growth in dinosaurs. *C R Acad Sci III-Vie* **323**, 543–550.

Cerda IA, Tambussi CP, Degrange FJ (2015) Unexpected microanatomical variation among Eocene Antarctic stem penguins (Aves: Sphenisciformes). *Hist Biol* **27**, 549–557.

Chatterjee S (2002) The morphology and systematics of *Polarornis*, a Cretaceous loon (Aves: Gaviidae) from Antarctica. In: *Proceedings of the 5th Symposium of the Society of Avian Paleontology and Evolution, Beijing, 1–4 June 2000*. (eds Zhou Z, Zhang F), pp. 125–155. Beijing, China: Science Press.

Chinsamy A, Martin LD, Dodson P (1998) Bone microstructure of the diving *Hesperornis* and the volant *Ichthyornis* from the Niobrara Chalk of western Kansas. *Cret Res* **19**, 225–235.

Chinsamy-Turan A (2005) *The Microstructure of Dinosaur Bone: Deciphering Biology with Fine-Scale Techniques*. Baltimore, MD: Johns Hopkins University Press.

Cubo J, Le Roy N, Martinez-Maza C, et al. (2012) Paleohistological estimation of bone growth rate in extinct archosaurs. *Paleobiology* **38**, 335–349.

Domning DP, de Buffrénil V (1991) Hydrostasis in the Sirenia: quantitative data and functional interpretations. *Mar Mamm Sci* **7**, 331–368.

Dutton AL, Lohmann KC, Zinsmeister WJ (2002) Stable isotope and minor element proxies for Eocene climate of Seymour Island, Antarctica. *Paleoceanography* **17**, 1016.

Dyke GJ, van Tuinen M (2004) The evolutionary radiation of modern birds (Neornithes): reconciling molecules, morphology and the fossil record. *Zool J Linn Soc* **141**, 153–177.

Enlow DH (1962) A study of the post-natal growth and remodeling of bone. *Am J Anat* **110**, 79–101.

Falke KJ, Hill RD, Qvist J, et al. (1985) Seal lungs collapse during free diving: evidence from arterial nitrogen tensions. *Science* **229**, 556–558.

Feduccia A (1999) *The Origin and Evolution of Birds*. New Haven, CT: Yale University Press.

Felts WJL, Spurrell FA (1965) Structural orientation and density in cetacean humeri. *Am J Anat* **116**, 171–203.

Francillon-Vieillot H, de Buffrénil V, Castanet J, et al. (1990) Microstructure and mineralization of vertebrate skeletal tissues. In: *Skeletal Biomineralization: Patterns, Processes and Evolutionary Trends*, Vol. 1. (ed. Carter JG), pp. 471–530. New York, NY: Van Nostrand Reinhold.

Germain D, Laurin M (2005) Microanatomy of the radius and lifestyle in amniotes (Vertebrata, Tetrapoda). *Zool Scr* **34**, 335–350.

Girondot M, Laurin M (2003) Bone Profiler: a tool to quantify, model, and statistically compare bone-section compactness profiles. *J Vertebr Paleontol* **23**, 458–461.

Groscolas R (1986) Changes in body mass, body temperature, and plasma fuel levels during the natural breeding fast in male and female emperor penguins, *Aptenodytes forsteri*. *J Comp Physiol B* **156**, 521–527.

Habib M (2010) The structural mechanics and evolution of aquaflying birds. *Biol J Linn Soc* **99**, 687–698.

Habib MB, Ruff CB (2008) The effects of locomotion on the structural characteristics of avian limb bones. *Zool J Linn Soc* **153**, 601–624.

Halsey LG, Butler PJ, Blackburn TM (2006) A phylogenetic analysis of allometry of diving. *Am Nat* **167**, 267–287.

Hayashi S, Houssaye A, Nakajima Y, et al. (2013) Bone inner structure suggests increasing aquatic adaptations in Desmostylia (Mammalia, Afrotheria). *PLoS ONE* **8**, e59146.

Houssaye A (2009) "Pachyostosis" in aquatic amniotes: a review. *Integr Zool* **4**, 325–340.

Jadwiszczak P (2001) Body size of Eocene Antarctic penguins. *Pol Polar Res* **22**, 147–158.

Jadwiszczak P (2006) Eocene penguins of Seymour Island, Antarctica: taxonomy. *Pol Polar Res* **27**, 3–62.

Kaiser G (1966) Functional anatomy of breathing and balance in seacows (Sirenia). *Anat Rec* **55**, 246.

Kolb C, Sánchez-Villagra M, Scheyer T (2011) The palaeohistology of the basal ichthyosaur *Mixosaurus* Baur, 1887 (Ichthyopterygia, Mixosauridae) from the Middle Triassic: palaeobiological implications. *C R Palevol* **10**, 403–411.

Kooyman GL, Ponganis PJ (1998) The physiological basis of diving to depth: birds and mammals. *Annu Rev Phyisol* **60**, 19–32.

Kooyman GL, Schroeder JP, Denison DM, et al. (1972) Blood nitrogen tensions of seals during simulated deep dives. *Am J Physiol* **223**, 1016–1020.

Ksepka DT, Clarke JA (2010) The basal penguin (Aves: Sphenisciformes) *Perudyptes devriesi* and a phylogenetic evaluation of the penguin fossil record. *Bull Am Mus Nat Hist* **337**, 1–77.

Ksepka DT, Bertelli S, Giannini NP (2006) The phylogeny of the living and fossil Sphenisciformes (penguins). *Cladistics* **22**, 412–441.

Ksepka DT, Clarke JA, DeVries TJ, et al. (2008) Osteology of *Icadyptes salasi*, a giant penguin from the Eocene of Peru. *J Anat* **213**, 131–147.

Ksepka DT, Fordyce RE, Ando T, et al. (2012) New fossil penguins (Aves: Sphenisciformes) from the Oligocene of New Zealand reveal the skeletal plan of stem penguins. *J Vert Paleo* **32**, 235–254.

Livezey BC, Zusi RL (2006) Higher-order phylogenetics of modern Aves based on comparative anatomy: I. Methods and characters. *Bull Carn Mus Nat Hist* **37**, 1–544.

Lovvorn JR, Croll DA, Liggins GA (1999) Mechanical versus physiological determinants of swimming speeds in diving Brünnich's Guillemots. *J Exp Biol* **202**, 1741–1752.

de Margerie E (2006) Fonction biomécanique des microstructures osseuses chez les oiseaux. *C R Palevol* **5**, 619–628.

de Margerie E, Cubo J, Castanet J (2002) Bone typology and growth rate: testing and quantifying "Amprino's rule" in the mallard (*Anas platyrhynchos*). *C R Biol* **325**, 221–230.

de Margerie E, Robin J-P, Verrier D, et al. (2004) Assessing a relationship between bone microstructure and growth rate: a fluorescent labeling study in the king penguin chick (*Aptenodytes patagonicus*). *J Exp Biol* **207**, 869–879.

Marples BJ (1952) Early Tertiary penguins of New Zealand. *N Z Geol Surv Paleontol Bull* **20**, 1–66.

Mayr G (2005) Tertiary plotopterids (Aves, Plotopteridae) and a novel hypothesis on the phylgenetic relationships of penguins (Spheniscidae). *J Zool Syst Evol Res* **43**, 61–71.

Mayr G, Gorobets L, Zvonok E (2013) The tarsometatarsus of the Middle Eocene loon *Colymbiculus udovichenkoi*. In: *Paleornithological Research 2013 – Proceedings of the 8th International Meeting of the Society of Avian Paleontology and Evolution*. (eds Göhlich UB, Kroh A), pp. 17–22. Vienna, Austria: Natural History Museum Vienna.

Meier PS, Bickelmann C, Scheyer TM, et al. (2013) Evolution of bone compactness in extant and extinct moles (Talpidae): exploring humeral microstructure in small fossorial mammals. *BMC Evol Biol* **13**, 55.

Meister W (1962) Histological studies of the long bones of penguins. *Anat Rec* **143**, 377–382.

Montes L, Castanet J, Cubo J (2010) Relationship between bone growth rate and bone tissue organization in amniotes: first test of Amprino's rule in a phylogenetic context. *Anim Biol* **60**, 25–41.

Myrcha A, Jadwiszczak P, Tambussi CP, et al. (2002) Taxonomic revision of Eocene Antarctic penguins based on tarsometatarsal morphology. *Pol Polar Res* **23**, 5–46.

Newell-Morris L, Sirianni JE (1982) Parameters of bone growth in the fetal and infant macaque (*Macaca nemestrina*) humerus as documented by trichromatic bone labels. In: *Factors and Mechanisms Influencing Bone Growth*. (eds Dixon AD, Sarnat BG), pp. 243–258. New York, NY: Alan R. Liss.

Nopcsa F (1923) Vorläufige notiz über die pachyostose und osteosklerose einiger mariner wirbeltiere. *Anat Anz* **56**, 352–359.

Olson SL (1977) Great Auk, *Pinguinis*, from the Pliocene of North Carolina (Aves: Alcidae). *Proc Biol Soc Wash* **90**, 690–697.

Olson SL, Hasegawa Y (1979) Fossil counterparts of giant penguins from the North Pacific. *Science* **206**, 688–689.

Padian K, de Ricqlès A, Horner JR (2001) Dinosaurian growth rates and bird origins. *Nature* **412**, 405–408.

Payton CG (1934) The position of the nutrient foramen and the direction of the nutrient canal in the long bones of the madder-fed pig. *J Anat* **68**, 500–510.

Pereira SL, Baker AJ (2008) DNA evidence for a Paleocene origin of the Alcidae (Aves: Charadriiformes) in the Pacific and multiple dispersals across northern oceans. *Mol Phylog Evol* **46**, 430–445.

Piatt JF, Nettleship DN (1985) Diving depths of four alcids. *Auk* **102**, 293–297.

Ponganis PJ, Meir JU, Williams CL (2011) In pursuit of Irving and Scholander: a review of oxygen store management in seals and penguins. *J Exp Biol* **214**, 3325–3339.

Porębski SJ (1995) Facies architecture in a tectonically-controlled incised-valley estuary: La Meseta Formation (Eocene) of Seymour Island, Antarctic Peninsula. *Stud Geol Pol* **107**, 7–97.

Prévost J (1961) *Ecologie du manchot emperor*. Paris: Hermann.

Rhodin AGJ (1985) Comparative chondro-osseous development and growth of marine turtles. *Copeia* **1985**, 752–771.

Rhodin AGJ, Ogden JA, Conlogue GJ (1981) Chondro-osseous morphology of *Dermochelys coriacea*, a marine reptile with mammalian skeletal features. *Nature* **290**, 244–246.

de Ricqlès A (1975) Recherches paléohistologiques sur les os longs des tétrapodes VII. – Sur la classification, la signification fonctionnelle et l'histoire des tissus oseux des tétrapodes. Première partie, structures. *Ann Paléontol* **61**, 51–129.

de Ricqlès A, de Buffrénil V (2001) Bone histology, heterochronies and the return of tetrapods to life in water: where are we? In: *Secondary Adaptation of Tetrapods to Life in Water*. (eds Mazin J-M, de Buffrénil V), pp. 289–310. München: Verlag Dr. Friedrich Pfeil.

Ridgway SH, Howard R (1979) Dolphin lung collapse and intramuscular circulation during free diving: evidence from nitrogen washout. *Science* **206**, 1182–1183.

Sato K, Shiomi K, Watanabe Y, et al. (2010) Scaling of swim speed and stroke frequency in geometrically similar penguins: they swim optimally to minimize cost of transport. *Proc R Soc Lond B Biol Sci* **277**, 707–714.

Sheldon A (1997) Ecological implications of mosasaur bone microstructure. In: *Ancient Marine Reptiles*. (eds Callaway JM, Nicholls EL), pp. 333–354. San Diego, CA: Academic Press.

Sigogneau-Russell D (1981) Etude ostéologique du reptile *Simoedosaurus* (Choristodera). IIe Partie: squelette postcranien. *Ann Paleontol* **67**, 61–140.

Simpson GG (1946) Fossil penguins. *Bull Am Mus Nat Hist* **87**, 7–99.

Slack KE, Jones CM, Ando T, et al. (2006) Early penguin fossils, plus mitochondrial genomes, calibrate avian evolution. *Mol Biol Evol* **23**, 1144–1155.

Smith NA (2011) Systematics and evolution of extinct and extant Pan-Alcidae (Aves, Charadriiformes): combined phylogenetic analyses, divergence estimation, and paleoclimatic interactions. Doctoral Dissertation, University of Texas, Austin.

Smith NA, Clarke JA (2014) Osteological histology of the Pan-Alcidae (Aves, Charadriiformes): correlates of wing-propelled diving and flightlessness. *Anat Rec* **297**, 188–199.

Stonehouse B (1960) The king penguin *Aptenodytes patagonicus* of South Georgia I. Breeding behavior and development. *Sci Rep Falkl Isl Depend Surv* **23**, 1–81.

Straehl FR, Scheyer TM, Forasiepi AM, et al. (2013) Evolutionary patterns of bone histology and bone compactness in Xenarthran mammal long bones. *PLoS ONE* **8**, e69275.

Taylor MA (2000) Functional significance of bone ballast in the evolution of buoyancy control strategies by aquatic tetrapods. *Hist Biol* **14**, 15–31.

Turvey ST, Green OR, Holdaway RN (2005) Cortical growth marks reveal extended juvenile development in New Zealand moa. *Nature* **435**, 940–943.

Wall WP (1983) The correlation between high limb-bone density and aquatic habits in recent mammals. *J Paleontol* **57**, 197–207.

Wienecke B, Robertson G, Kirkwood R, et al. (2007) Extreme dives by free-ranging emperor penguins. *Polar Biol* **30**, 133–142.

Williams TD (1995) *The Penguins*. Oxford: Oxford University Press.

Wilson EA (1907) Aves. *British Natural Antarctic Expedition (1901–1904) Reports* **2**, 1–21.

Wilson LE, Chin K (2014) Comparative osteohistology of *Hesperornis* with reference to pygoscelid penguins: the effects of climate and bahviour on avian bone microstructure. *R Soc Open Sci* **1**, 140245.

Yury-Yáñez RE, Ossa L, Rubilar-Rogers D, et al. (2012) Inferring growth in giant penguins from the Paleogene of Antarctica and the Neogene of South America. Abstracts of the 72nd Annual Meeting of the Society of Vertebrate Paleontology, 99.